Cement & Concrete Composites 45 (2014) 209–226

Contents lists available at ScienceDirect

Cement & Concrete Composites

journal homepage: www.elsevier.com/locate/cemconcomp

Linking fresh and durability properties of paste to SCC mortar

Helena Figueiras [a,*], Sandra Nunes [a], Joana Sousa Coutinho [a], Carmen Andrade [b]

[a] LABEST – Laboratory for Concrete Technology and Structural Behaviour, Faculdade de Engenharia, Universidade do Porto, Rua Dr. Roberto Frias, 4200-465 Porto, Portugal
[b] CISDEM – Center for Durability and Safety of Structures and Materials, C/Serrano Galvache No. 4, 28033 Madrid, Spain

ARTICLE INFO

Article history:
Received 3 November 2012
Received in revised form 11 September 2013
Accepted 22 September 2013
Available online 29 September 2013

Keywords:
Self-compacting concrete
Paste
Mortar
Statistical factorial design
Fresh and durability properties

ABSTRACT

In the last years many approaches to design SCC have been developed, but it remains a very complex process since it is necessary to manipulate several variables and understand their effects on concrete behaviour (fresh and hardened state). The prediction of concrete or mortar behaviour based on paste properties will be a significant contribution to simplify SCC design. With this purpose, two statistical experimental designs were carried out, one at paste level and the other at mortar level, to mathematically model the influence of mixture parameters on fresh and durability properties. The derived numerical models were used to define an area, labelled by self-compacting zone at paste level (SCZ), where fresh properties of the paste enable the design of SCC mortar. Furthermore, in order to extend this link to durability properties, the effect of including aggregate in cement paste was evaluated by means of the electrical resistivity test.

1. Introduction

Durability of concrete structures is presently looked at with great concern as it represents a challenge to achieve sustainable development in construction. Self-compacting concrete (SCC), initially developed in Japan, corresponds to an advanced special concrete type as it leads to technological, economic and environmental benefits. The main advantage of this sustainable technology lies in the unneeded compaction during placing, thus leading to a homogeneous and more durable material. In the fresh state, SCC must show filling ability, resistance to segregation and passing ability [1]. The selection of constituent materials and the design of mix proportions are essential factors to achieve adequate fresh properties. To produce SCC, a good balance between deformability and resistance to segregation has to be accomplished, which can be made possible by the use of chemical admixtures (superplasticizers, viscosity agents, etc.) combined with high concentrations of fine particles (cement and mineral admixtures) [2]. In addition, the characteristics of fine and coarse aggregate are also very important. With the growing variety of materials available to produce concrete, the mix design process has become complex since it is necessary to manipulate several variables and their interaction is difficult to predict. Indeed, to achieve the adequate performance in fresh and hardened states further work is needed to better understand the effect of mixture parameters governing material performance [3].

Several different mix-design methods have been developed by many academic institutions and construction industry companies, but still, there is no standard method for SCC mix design [1]. Typically, mixture optimization is based on a trial an error approach where each parameter is changed one at a time to assess its influence on concrete properties. This process does not permit understanding interactions of the mixture parameters, may involve carrying out a large and unpredictable number of trial batches and does not guarantee an optimal general solution. One of the methodologies that lately has been applied in the SCC mix design is the statistical experimental design. The derived statistical models established on the basis of a factorial design, highlight not only significance of the mixture parameters but also their interactions on concrete properties. Using such numerical models, a multi-parametric optimization can be carried out, with the user controlling the goal of the optimization and the significance of each experimental parameter. In fact, this approach increases the efficiency in selecting the optimum mix proportions for a given set of constraints (related to fresh and hardened properties and economic constraints) based on a limited number of experimental data points [3–5]. An additional advantage of the factorial experimental design is that there is some freedom to define the mixture parameters (it can be applied to paste, mortar or concrete) and to select the responses to be analysed (e.g. rheological parameters, empirical fresh tests results, durability properties, etc.) [6]. This mix-design approach was followed in the present work.

* Corresponding author. Tel.: +351 918452233; fax: +351 225081835.
E-mail addresses: hfig@fe.up.pt (H. Figueiras), snunes@fe.up.pt (S. Nunes), jcouti@fe.up.pt (J.S. Coutinho), andrade@ietcc.csic.es (C. Andrade).

0958-9465/$ - see front matter © 2013 Published by Elsevier Ltd.
http://dx.doi.org/10.1016/j.cemconcomp.2013.09.020

Several different design methods found in the literature consider SCC as a suspension of aggregates in paste, separating optimization of the granular skeleton grading, paste volume and paste composition. In fact, paste plays a major role in concrete workability and therefore it is reasonable to expect that there is a direct relationship between paste and concrete flow behaviour [7]. The prediction of the concrete behaviour based on paste properties facilitates the design of SCC, reduces the volume of material required for testing and takes advantage of greater accuracy and precision of paste rheology tests [7,8]. The rheological behaviour of cement paste is controlled by the same factors that control any other suspension, namely, by macro-level factors like particle size, size distribution, shape, texture, density, water content, etc., and by micro-level forces such as colloidal, Brownian and viscous forces. Depending on the size of the particles, on their volume fraction in the mixture and on external forces (applied stress or strain rate), one or several of these interactions dominate (referred by Flatt [9]). Colloidal particles forces dominate, to a large extent, the complex and time dependent behaviour of cement paste, while for most aggregate sizes, only viscous forces are relevant [6]. According to Wallevik and Wallevik [10] rheology of fresh concrete or mortar is much simpler than rheology of cement paste, due to the fact that the time-dependent behaviour (thixotropy and structural breakdown) is more pronounced in cement paste because of the absence of aggregates, which act as a very effective grinder and or dispersant.

The objective of this paper is therefore to establish a link between paste and mortar which exhibit adequate fresh properties (deformability and viscosity) to produce self-compacting concrete. Furthermore, in order to extend this link to durability properties, the effect of including aggregate in cement paste was evaluated by means of the electrical resistivity test. With this purpose, two statistical experimental designs were conducted, with the same set of materials, one at paste level and the other at mortar level (including reference sand). At paste level, numerical models were established relating mixture parameters to rheological properties (yield stress and plastic viscosity), empirical fresh properties (flow diameter and free water content) and a durability property (electrical resistivity). At mortar level empirical fresh properties (flow diameter and flow time), a mechanical property (compressive strength) and the same durability property evaluated in paste (electrical resistivity) were assessed. The mortar numerical models were used to find optimal solutions that satisfy SCC fresh requirements, i.e. to determine the range of mortar mixture parameters where deformability and viscosity coexist in a balanced manner. By using the mixture parameters of the optimized mortars and the derived numerical models to describe paste properties, it was possible to define an area, labelled by self-compacting zone [11,12] at paste level, where the rheological properties of the paste enable the design of a self-compacting mortar. Furthermore, the influence of the aggregate in the electrical resistivity of mortar was studied, which allowed to draw contour plots that aid in the design of SCC mortar with defined durability requirements, based on tests at paste level only. Additionally the correlation between rheological and empirical tests results was discussed and the evolution of paste rheological behaviour during the hydration process was assessed.

2. Experimental programme

2.1. Materials characterization

The mortar and paste mixes investigated in this study were prepared with ternary mixtures including white cement (CEM II/A-L 52.5N according to EN 197-1 [13]) and two mineral additions, metakaolin and limestone filler. The chemical composition and some physical properties of the cement and the two mineral additions are presented in Table 1. The particle size distribution performed by a laser diffraction granulometer is shown in Fig. 1. A polycarboxylate type high range water reducing admixture was used having a specific gravity of 1.07 and 26.5% solid content. In mortar mixes a reference sand was employed, conforming to EN 196-1 [14]. Reference sand used is a siliceous round natural sand (0.08–2 mm) with a specific gravity of 2.63 and an absorption value of 0.30%. Distilled water was used for all paste and mortar mixes.

2.2. Experimental design

The experiments were designed according to a statistical design approach known as two-level factorial design (2^k). This is a process of planning experiments in order to collect appropriate data that can be analyzed by statistical tools, such as analysis of variance, resulting in a valid basis for deriving an empirical numerical model that expresses the relationship between the input variables (e.g. mixture parameters) and response variables (e.g. fresh or hardened properties of paste/mortar). Factorial design is frequently used in experiments involving large number of parameters (input variables) and when it is important to study not only the isolated significance of each parameter in response but also their interaction [15]. According to studies conducted by some authors [4,16–18] the response surface of mortar and paste properties, fresh and hardened properties, exhibit some curvature, therefore, in this study experiments were designed according to a factorial central composite design adequate to fit a second order model. The generic form of a second order model is:

$$y = \beta_0 + \sum_{i=1}^{k} \beta_i x_i + \sum_{i=1}^{k} \beta_{ii} x_i^2 + \sum_{i<j} \sum \beta_{ij} x_i x_j + \varepsilon \quad (1)$$

where y is the response of the material; x_i are the independent variables; β_0 is the independent term; β_i, β_{ii} and β_{ij} are the coefficients of independent variables and interactions, representing their contribution to the response and ε is the random residual error term representing the effects of variables or higher order terms not considered in the model.

To define paste composition, four independent variables x_i were selected, namely, water to powder volume ratio (V_w/V_p), water to cement weight ratio (w/c), superplasticizer to powder weight ratio (S_p/p) and metakaolin to cement weight ratio (mtk/c). For mortar mixtures it was necessary to include an additional variable to define the composition completely, which was sand to mortar volume ratio (V_s/V_m). The selection of these parameters, used widespread in the design of SCC mixtures, was based on the method developed by Okamura et al. [2]. A complete 2^4 factorial statistical design, corresponding to four factors at two levels, was selected for the studies carried out at paste level whereas for the study of mortar mixes a 2^{5-1} fractional factorial statistical design was adopted. The fractional factorial design was selected for mortar experimental design since it involves fewer runs than the complete set of $2^5 = 32$ runs, while it can still be used to obtain information on the main effects and on the two-factor interactions. Axial points and central points were added to both experimental designs (Central Composite Design), allowing, thereby a second-order model fitting. The effect of each factor was evaluated at five different levels, codified in $-\alpha$, -1, 0, $+1$, $+\alpha$. In order to make the design rotatable (i.e. the standard deviation of the predicted response is constant in all points at the same distance from the centre of the design) the α value should be taken equal to $n_f^{1/4}$, where n_f is the number of points in the factorial part of the design [5] [15]. The absolute value of each variable corresponding to a given level

Table 1
Chemical and physical properties of the cement, metakaolin and limestone filler.

	CEM II/A-L 52.5N (white)[a]	Metakaolin	Limestone filler[a]
SiO_2 (%)	18.80	52.00	–
Al_2O_3 (%)	2.23	45.00	–
Fe_2O_3 (%)	0.20	0.46	0.02
CaO (%)	66.42	<0.50	–
MgO (%)	0.66	<0.50	–
SO_3 (%)	2.17	<0.10	–
Na_2O (%)	–	<0.50	–
Na_2O_{eq} (%)	0.30	–	–
$CaCO_3$ (%)	–	–	99.00
$MgCO_3$ (%)	–	–	0.30
K_2O (%)	–	<0.50	–
TiO_2	–	1.50	–
MnO	–	<0.30	–
P_2O_5	–	<0.30	–
Cl^- (%)	0.03		<0.001
S^{2-} (%)	–		<0.04
Loss on ignition (%)	8.60	1.50	43.10
Insoluble residue (%)	0.31	61	0.20
Specific density (g/cm^3)	3.04	2.21	2.68
Blaine (cm^2/g)	5011	31678	5150
Residue, 90 μm (%)	0.00	0.00	0.01
Residue, 45 μm (%)	1.80	1.09	2.44
Residue, 32 μm (%)	7.38	2.55	4.41
Mean size (μm)	11.03	7.12	6.53
Vicat test			
Initial set (min.)	154	–	–
Final set (min.)	214	–	–

[a] Information provided by the supplier.

depends on the variable itself and the specific experimental plan. For a given variable and a given experimental plan the transformation of coded into absolute values is of the form:

$$a = a_0 + x \cdot \Delta a \tag{2}$$

with a being the absolute value in normal units; a_0 being the absolute value of the variable at the centre of the design; x being the coded variable measured with the step like units and Δa the variable variation (in absolute values) corresponding to a unit change in the coded variable. The range of variables variation ($-\alpha$ to $+\alpha$) was established based on a set of preliminary tests where extreme mixtures, in terms of fresh state behaviour, were searched (least fluid mixture and most fluid mixture), but ensuring performance of characterization testing. Experimental programs also included central point replication in order to evaluate the experimental error associated to conditions and test procedures variability (six replicate central runs were prepared) [15]. Table 2 presents the experimental plans adopted to study paste (PED) and mortar (MED) mixtures.

SCC mix proportions are generally established based on the volumetric composition of the mix, due to the SCC core concept of overfilling the voids between the aggregate skeleton [1]. Mix proportions of paste and mortar prepared in this study were obtained using the formulation presented in the Appendix.

2.3. Response variables

Given the main objectives of this study, the selected response variables (y) of the paste experimental plan (PED) were: flow diameter ($D_{flow,paste}$), free water content (w_{free}), yield stress at 10 min ($\tau_{0,10min}$), plastic viscosity at 10 min ($\eta_{pl,10min}$), yield stress at 23 min ($\tau_{0,23min}$), plastic viscosity at 23 min ($\eta_{pl,23min}$) and resistivity at 28 days ($\rho_{28d,paste}$). In the mortar experimental plan (MED) assessed response variables were: flow diameter ($D_{flow,mortar}$), flow time with the V-funnel test ($T_{funnel,mortar}$), resistivity at 28 days ($\rho_{28d,mortar}$) and compressive strength at 28 days (fc_{28d}). A brief explanation of the tests performed on paste and mortar is presented below.

2.3.1. Paste test methods

2.3.1.1. Paste flow test. The deformability of paste was assessed by the paste flow test, also known as mini-slump flow test. This test is carried out by using a truncated cone with 19 mm top diameter, 38 mm lower diameter and 57 mm height [19]. After filling the cone and lifting it vertically to let the paste flow freely, the paste flow diameter ($D_{flow,paste}$) was taken as the average of two perpendicular diameters of the spread area.

2.3.1.2. Centrifugal consolidation test. The centrifugal consolidation test was used to determine the free water of the paste, i.e. the water that is not restricted by particles and can move around them [20,21]. The paste is poured into four plastic containers of the centrifuge equipment (approximately 30 ml on each container) and centrifuging was carried out at 3500 rpm during 15 min. After the centrifugal cylinder separation, the particles in the paste are compacted and the free water rises up to the surface of the paste, and is, then, removed with a pipette. The weight of the containers before and after centrifuging was determined. The free water content (w_{free}) was calculated from,

$$w_{free} = \frac{w_{final} - w_{initial}}{V_{paste}} \tag{3}$$

where $w_{initial}$ and w_{final} are the weight of containers before and after removing the surplus of water, respectively and V_{paste} the volume of

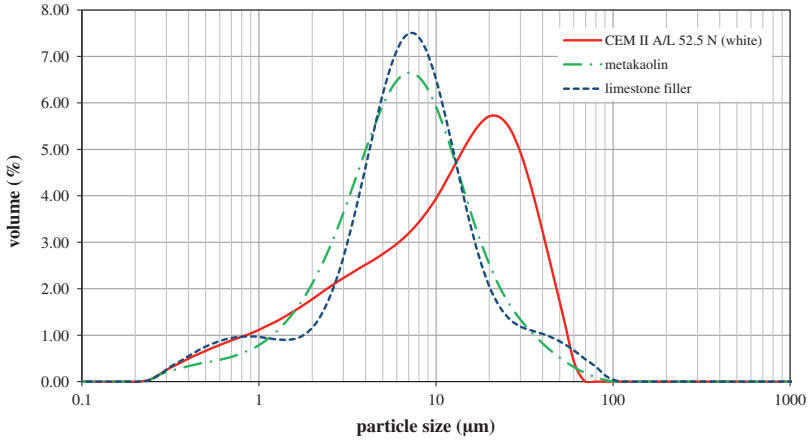

Fig. 1. Particle size distribution curves of cement, metakaolin and limestone filler, in terms of volume.

Table 2
Experimental designs characterization.

Designation	Experimental design	Independent variables	$[-\alpha;+\alpha]$
Paste experimental design (PED)	2^4	V_w/V_p	[0.783; 0.904]
	$\alpha = 2.000$	w/c	[0.364; 0.440]
	$n_c = 6$	S_p/p	[0.682%; 0.724%]
	$n_f = 16$	mtk/c	[6.44%; 10.89%]
	$n_a = 8$		
Mortar experimental design (MED)	2^{5-1}	V_w/V_p	[0.800; 1.000]
	$\alpha = 2.000$	w/c	[0.360; 0.460]
	$n_c = 6$	S_p/p	[0.680%; 0.720%]
	$n_f = 16$	mtk/c	[3.00%; 15.00%]
	$n_a = 10$	V_s/V_m	[0.400; 0.500]

n_c: Number of central points; n_f: number of factorial points; n_a: number of axial points.

paste on each container. A strong relation between paste flow time assessed by the marsh cone flow test and free water content (centrifuge test) was found by Nunes et al. [22]. Therefore, the centrifugal consolidation test is a promising substitute test of the Marsh cone with the advantage of being equally precise for lower and higher fluidity paste.

2.3.1.3. Rheological test. The rheological flow behaviour of viscoplastic non-Newtonian fluids such as cement paste is often characterized by the yield stress (τ_0) and plastic viscosity (η_{pl}), in accordance with the Bingham model. More complex analytical rheological models have been applied to characterize cement paste behaviour with different degrees of success. In general, the use of the Bingham model offers a less favourable fitting for highly pseudoplastic mixtures or for tests performed in a wide range of shear rates, due to the weakness to fit the nonlinear portion of the flow curve observed at low shear rates [23,24]. Despite all the shortcomings of the Bingham equation, it is still the most used method on account of its simplicity (a low number of adjustable parameters). In the present study, the Bingham model was selected to fit the flow curve data. According to this model, the relationship between shear stress and shear rate is of the form (Eq. (4)),

$$\tau = \tau_0 + \eta_{pl}\dot{\gamma} \tag{4}$$

where τ (in Pa) is the shear stress applied to the material, τ_0 is the yield stress (in Pa), η_{pl} (in Pa s) is the plastic viscosity, and $\dot{\gamma}$ (in s^{-1}) is the shear strain rate. The yield stress corresponds to the minimum required shear stress to initiate flow, while the plastic viscosity measures the resistance of the paste to flow under external stress.

Rheological tests were carried out with a rotational rheometer, using a cone and plate geometry measuring device (cone with 40 mm diameter and 4° angle, providing a gap of 150 μm). This geometry measuring device has the major advantage of imposing a constant shear rate through the entire sample, important in the case of time-dependent and non-Newtonian fluids such as cement paste [25]. However, according to Chhabra and Richardson [25] the use of cone and plate tool may be subject to some criticism, especially due to limitations of the maximum particle size. For this geometry (cone and plate 4°/40 mm) the corresponding gap size is 150 μm, allowing for a maximum particle size of 15 μm. The gap size must be at least 10 times larger than the mean particles size [26], and this may conflict with the gap size required to ensure near constant shear rate. As can be observed in Table 1, the coarser powder materials have few particles with sizes as high as 35 μm, and the mean particle size is lower than 15 μm. Furthermore, a superplasticizer was always included preventing the formation of large floccules.

A viscometry shear stepped test in shear rate control mode with controlled temperature (25 ± 0.1 °C) was implemented to obtain equilibrium flow curves. The rheometer was programmed to perform a 12-step logarithmic increase of shear rate ranging from 0.1 to 200 s^{-1} and back again to complete a full cycle. The complete testing sequence is illustrated in Fig. 2a. The descending part of the obtained flow curves were fitted to the Bingham model (see Eq. (4)) and the adjusted model parameters, τ_0 and η_{pl}, were taken as the rheological test results for the present study. An example of the up- and down-flow curves of a cement paste tested in this study is presented in Fig. 2b.

An important feature of cement paste flow behaviour is the extent of hysteresis that is generally observed between the up and down flow curves in a shear ramp test. This hysteresis reflects a reversible time-dependent behaviour of cementitious materials, called thixotropy. In the present study, thixotropy effects were mitigated, as can be observed in Fig. 2b by appropriate pre-conditioning of samples (pre-shear was applied to the sample during 45 s at a shear rate of 200 s^{-1}), shear stepped test and using only the down-curve data to adjust model parameters. A more detailed description of the measuring sequence setup and the procedure used to fit the flow-curves by the Bingham model is given in Nunes et al. [22].

2.3.1.4. Paste electrical resistivity at 28 days. Electrical resistivity is an intrinsic property of the material that relates to the ability of cement paste to carry electric charge and it depends mainly on the hydration process (nature and topography of the pore structure), changes in pore solution composition and moisture and temperature conditions. Electrical resistivity was assessed by the two electrodes technique on cubic specimens ($40 \times 40 \times 40$ mm^3) in which stainless steel meshes were embedded to work as electrodes. Applying Ohm's Law, as shown in Eq. (5), the relationship between the intensity of the applied current and the potential difference measured, gives the electrical resistance of the material. The resistivity is obtained applying to the electrical resistance a geometric factor, which depends on the geometrical dimensions of the specimen and the electrodes used.

$$R = \frac{V}{I} = \rho \cdot \left(\frac{L}{A}\right) \Rightarrow \rho = \frac{V \cdot A}{L \cdot I} \tag{5}$$

where R is the electric resistance, (Ω); I, current (A); V, voltage (V); ρ, electric resistivity (Ω m); L, length between electrodes (m); and A (m^2) the cross area of the test specimen through which current passes. The measurement was carried out at 28 days old paste ($\rho_{28d,paste}$). Paste cubes were demoulded one day after casting and kept under water in a chamber under controlled environmental conditions (Temp. = 20 °C) until testing. Since all the specimens were at the same moisture (saturated) and temperature conditions, resistivity can be used to compare the porous structure of various paste specimens and therefore, constitute a measure of the amount and interconnectivity of the cementitious matrix pores.

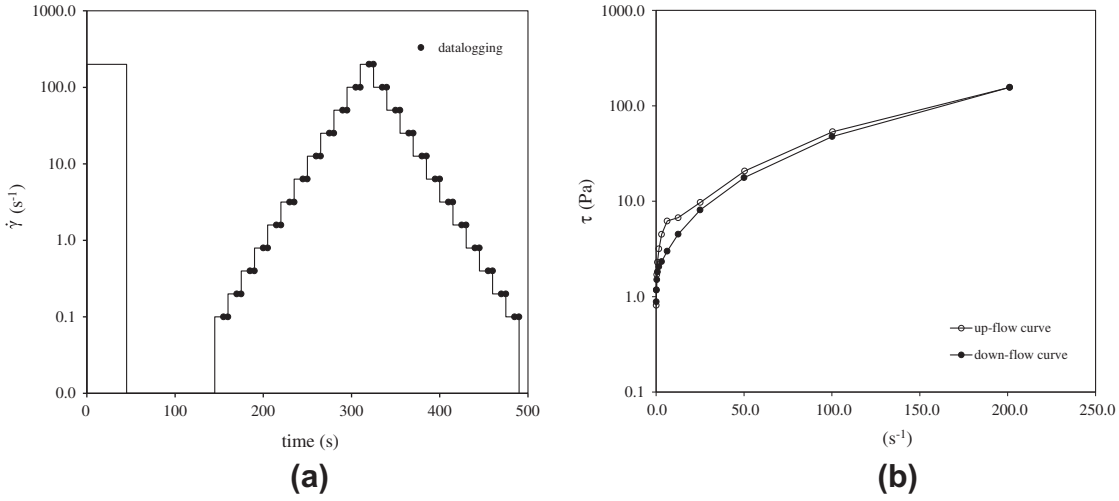

Fig. 2. (a) Testing sequence for the rheological tests and (b) up- and down-flow curves of a cement paste.

In fact, according to Andrade [27], electrical resistivity of water saturated specimens provides indications on the pore connectivity and therefore, on the concrete resistance to penetration of liquid or gas substances, thus resistivity is a parameter which accounts for the main key properties related to concrete durability. Regarding the influence of the chemical composition of the pore solution, Andrade [27] stated that its impact in the total resistivity is small providing concrete remains alkaline. At high pH values the pore solution resistivity varies from 0.3 to 1.0 Ω m, which is comparatively very small taking into account that mortar resistivity after several days of hardening is in the range of few dozen Ω m. Rajabipour et al. [28] also found in their work that the pore connectivity, for saturated specimens, is the single most important parameter governing the overall conductivity of a cement paste specimen. However some authors [29] called attention to the fact that the replacement of Portland cement with supplementary cementing materials, such as silica fume, fly ash and ground blast furnace may have a significant effect on the electrical conductivity of pore solution, depending on the alkali content of the supplementary cementing material, replace level and age.

2.3.2. Mortar tests methods

2.3.2.1. Mortar flow and V-funnel tests. The mortar flow test ($D_{flow,mortar}$) was used to assess deformability by calculating the flow diameter as the mean of two diameters in the spread area and the V-funnel test ($T_{funnel,mortar}$) was used to assess the viscosity and passing ability of the mortar. The flow cone and the V-funnel used have the same internal dimensions as the Japanese equipment (see [2] for details on equipment and test procedures).

2.3.2.2. Mortar electrical resistivity and compressive strength at 28 days. Mortar resistivity ($\rho_{28d,mortar}$) was assessed at 28 days on prismatic specimens ($40 \times 40 \times 160$ mm^3), using the same technique used on paste specimens. Mortar specimens were demoulded one day after casting and kept under water in a chamber under controlled environmental conditions (Temp. = 20 °C) until testing. After completing the electrical resistivity test, a non-destructive test, the specimens were used to assess mortar compressive strength (fc_{28d}).

2.4. Mixing and testing sequence

Paste mixes were prepared in 0.31 l batches using a vertical paddle mixer, according to the following procedure: (i) powder materials were mixed with mixing water for 120 s at 750 rpm; (ii) superplasticizer was added and mixed during 120 s at 750 rpm; (iii) the mixer was stopped for 60 s and (iv) mixing was resumed for 120 s at 2000 rpm. Mortar mixes were prepared in 2.42 l batches and mixed in a two-speed mixer complying to EN 196-1:2005 [14]. The mixing sequence was as follows: (i) sand and powder materials were mixed with 0.80 of the mixing water during 60 s; (ii) the mixer was stopped to scrape material adhering to the mixing bowl and mixed for another 60 s; (iii) the rest of the water was added with the superplasticizer and mixed for 60 s; (iv) the mixer was stopped again to scrape material adhering to the bowl and mixed for 60 s; (v) the mixer was then stopped for 5 min and (vi) the mortar was mixed during a further 90 s. The mixer was always set at low speed except in the last 90 s of the mixing sequence where it was set as high speed (as defined in [14]). Mixtures (paste and mortar mixtures) from experimental plans were tested in a random order to reduce effects of extraneous variables not explicitly included in the experiment. Paste tests were performed according to the following sequence: (a) 0 min: paste mixing procedure was started; (b) 10 min: 1st rheological test in the rheometer; (c) 12 min: paste flow test; (d) 23 min: 2nd rheological test in the rheometer; (e) 26 min: centrifuge test and (f) 36 min: moulding of three cubic test specimens with embedded stainless steel meshes ($40 \times 40 \times 40$ mm^3). Mortar testing sequence was approximately the following: (a) 0 min: mortar mixing procedure was started; (b) 10 min: mortar flow test; (c) 15 min: mortar V-funnel test and (d) 17 min: moulding of three prismatic test specimens with embedded stainless steel meshes ($40 \times 40 \times 160$ mm^3). Before the beginning of each test the sample was re-mixed by hand with a paddle to destroy any structure formed during resting (thixotropic effects).

3. Discussion of results

3.1. Tests results

Test results of the mixes prepared in the PED and the MED are summarized in Tables 3 and 4, respectively. In the case of the MED it was not possible to perform the V-funnel test of mixture MCC10, due to the excessive viscosity of the mixture, and the electrical resistivity test of mixtures MC1 and MC5 was also not carried out, due to problems with the mesh embedded in the specimens.

An overall statistical analysis of the response variables, including minimum and maximum values, mean value, standard

Table 3
Coded values of the independent variables and fresh and hardened paste results.

Mix number	Ref.	V_w/V_p	w/c	S_p/p	mtk/c	$D_{flow,paste}$ (mm)	w_{free} (kg/m^3)	$\tau_{0,10min}$ (Pa)	$\eta_{pl,10min}$ (Pa s)	$\tau_{0,23min}$ (Pa)	$\eta_{pl,23min}$ (Pa s)	$\rho_{28d,paste}$ (Ω m)
1	PC1	0	0	0	0	191.0	59.25	0.240	0.240	1.084	0.283	68.7
2	PC2	0	0	0	0	208.5	63.42	0.231	0.234	1.140	0.272	68.8
3	PC3	0	0	0	0	197.3	67.17	0.210	0.222	0.946	0.270	72.0
4	PC4	0	0	0	0	200.8	66.08	0.259	0.225	1.090	0.275	75.4
5	PC5	0	0	0	0	206.0	63.67	0.197	0.242	1.330	0.248	65.6
6	PC6	0	0	0	0	204.5	62.75	0.208	0.242	1.036	0.301	72.7
7	PF1	−1	−1	−1	−1	194.8	57.56	0.294	0.264	1.398	0.305	68.4
8	PF2	1	−1	−1	−1	191.8	65.67	0.205	0.246	1.319	0.282	67.4
9	PF3	−1	1	−1	−1	210.8	69.33	0.098	0.205	0.547	0.232	53.2
10	PF4	1	1	−1	−1	209.3	74.08	0.101	0.177	0.672	0.206	51.7
11	PF5	−1	−1	1	−1	190.7	55.92	0.199	0.266	1.303	0.309	64.2
12	PF6	1	−1	1	−1	195.5	69.33	0.148	0.215	1.057	0.268	66.3
13	PF7	−1	1	1	−1	225.8	75.83	0.113	0.207	0.261	0.221	56.3
14	PF8	1	1	1	−1	205.3	83.08	0.071	0.164	0.244	0.185	62.6
15	PF9	−1	−1	−1	1	154.0	44.08	1.663	0.347	4.681	0.442	99.7
16	PF10	1	−1	−1	1	170.0	53.17	0.942	0.296	3.249	0.396	93.4
17	PF11	−1	1	−1	1	173.5	54.00	0.320	0.261	1.354	0.303	78.0
18	PF12	1	1	−1	1	192.8	66.25	0.271	0.224	1.385	0.278	69.7
19	PF13	−1	−1	1	1	163.5	45.08	1.335	0.279 (*)	4.407	0.449	97.1
20	PF14	1	−1	1	1	175.0	54.08	0.726	0.282	2.615	0.358	97.8
21	PF15	−1	1	1	1	190.3	57.83	0.267	0.263	1.470	0.255	76.4
22	PF16	1	1	1	1	201.5	72.83	0.145	0.217	0.779	0.227	74.8
23	PCC1	−2	0	0	0	184.5	52.67	0.328	0.286	2.110 (*)	0.364	76.0
24	PCC2	2	0	0	0	209.0	76.50	0.183	0.198	0.679	0.222	71.9
25	PCC3	0	−2	0	0	158.0	48.00	1.412	0.338	4.538	0.485	87.8
26	PCC4	0	2	0	0	198.5	75.83	0.130	0.200	0.471	0.226	60.5
27	PCC5	0	0	−2	0	193.5	61.83	0.230	0.255	1.264	0.295	76.8
28	PCC6	0	0	2	0	213.8	67.83	0.199	0.232	0.755	0.259	66.3
29	PCC7	0	0	0	−2	216.8	71.42	0.077	0.199	0.460	0.218	50.5
30	PCC8	0	0	0	2	156.8	46.83	1.120	0.319	3.596	0.402	102.8

(*) Observation identified as an outlier.

Table 4
Coded values of the independent variables and fresh and hardened mortar results.

Mix number	Ref.	V_w/V_p	w/c	S_p/p	V_s/V_m	mtk/c	$D_{flow,mortar}$ (mm)	$T_{funnel,mortar}$ (s)	fc_{28d} (MPa)	$\rho_{28d,mortar}$ (Ω m)
1	MC1	0	0	0	0	0	268.3	6.95	86.5	–(***)
2	MC2	0	0	0	0	0	297.5	6.10	89.6	168.5
3	MC3	0	0	0	0	0	270.8	7.31	90.2	167.2
4	MC4	0	0	0	0	0	269.8	6.97	86.2	165.5
5	MC5	0	0	0	0	0	275.8	6.68	79.5 (*)	–(***)
6	MC6	0	0	0	0	0	270.8	7.19	86.6	171.3
7	MF1	−1	−1	−1	−1	1	143.3	37.45	91.3	290.8
8	MF2	1	−1	−1	−1	−1	306.0	3.91	89.6	107.2
9	MF3	−1	1	−1	−1	−1	343.5	4.24	82.2	87.9
10	MF4	1	1	−1	−1	1	230.0	6.34	83.9	205.9
11	MF5	−1	−1	1	−1	−1	336.8	5.19	89.9	105.2
12	MF6	1	−1	1	−1	1	187.3	11.11	87.8	277.3
13	MF7	−1	1	1	−1	1	244.8	8.84	85.0	217.6
14	MF8	1	1	1	−1	−1	344.0	2.87	83.9	82.0
15	MF9	−1	−1	−1	1	−1	278.5	8.10	90.6	133.0
16	MF10	1	−1	−1	1	1	163.3	16.23	88.5	295.5
17	MF11	−1	1	−1	1	1	223.0	11.25	85.7	228.2
18	MF12	1	1	−1	1	−1	330.3	3.55	79.4	93.5
19	MF13	−1	−1	1	1	1	140.5	38.08	89.9	336.7
20	MF14	1	−1	1	1	−1	282.5	5.82	85.8	112.4
21	MF15	−1	1	1	1	−1	333.5	5.74	81.7	102.8
22	MF16	1	1	1	1	1	237.0	7.99	79.7	228.2
23	MCC1	−2	0	0	0	0	292.0	7.95	90.4	155.2
24	MCC2	2	0	0	0	0	273.5	4.56	83.1	154.5
25	MCC3	0	−2	0	0	0	210.8	11.00	93.4	247.9
26	MCC4	0	2	0	0	0	312.3	5.00	80.6	146.2
27	MCC5	0	0	−2	0	0	260.0	7.08	84.3	176.0
28	MCC6	0	0	2	0	0	305.0	5.73	84.5	158.0
29	MCC7	0	0	0	−2	0	307.8	5.34	84.0	158.3
30	MCC8	0	0	0	2	0	258.5	8.50	80.8	181.7
31	MCC9	0	0	0	0	−2	340.8	3.35	80.0	49.0
32	MCC10	0	0	0	0	2	101.8	–(**)	87.7	336.6

(*) Observation identified as an outlier.
(**) Test not performed due to excessive viscosity.
(***) Test not performed due to problems with the embedded mesh.

Table 5
Statistics of the results for the total points from PED and MED.

	Minimum	Maximum	Mean	Stand. deviation	Coeff. of variation (%)
Paste experimental design (PED)					
$D_{flow,paste}$ (mm)	154.0	225.8	192.8	18.6	9.7
w_{free} (kg/m^3)	44.08	83.08	62.71	10.18	16.2
$\tau_{0,10min}$ (Pa)	0.071	1.663	0.397	0.437	109.9
$\eta_{pl,10min}$ (Pa s)	0.164	0.347	0.244	0.045	18.3
$\tau_{0,23min}$ (Pa)	0.244	4.681	1.556	1.287	82.7
$\eta_{pl,23min}$ (Pa s)	0.185	0.485	0.295	0.077	26.0
$\rho_{28d,paste}$ (Ω m)	50.5	102.8	73.1	14.0	19.2
Mortar experimental design (MED)					
$D_{flow,mortar}$ (mm)	101.8	344.0	263.7	62.9	23.9
$T_{funnel,mortar}$ (s)	2.87	38.08	8.92	8.18	91.7
fc_{28d} (MPa)	79.4	93.4	85.9	3.8	4.5
$\rho_{28d,mortar}$ (Ω m)	49.1	336.7	178.0	75.6	42.5

Table 6
Spearman's correlation matrix within PED results.

	$D_{flow,paste}$	w_{free}	$\tau_{0,10\,min}$	$\eta_{pl,10\,min}$	$\tau_{0,23\,min}$	$\eta_{pl,23\,min}$	$\rho_{28d,paste}$
$D_{flow,paste}$	1.000	0.858	−0.858	−0.847	−0.880	−0.859	−0.810
w_{free}		1.000	−0.907	−0.965	−0.924	−0.941	−0.773
$\tau_{0,10\,min}$			1.000	0.888	0.933	0.906	0.880
$\eta_{pl,10\,min}$				1.000	0.929	0.929	0.773
$\tau_{0,23\,min}$					1.000	0.885	0.810
$\eta_{pl,23\,min}$						1.000	0.781
$\rho_{28d,paste}$							1.000

All correlations are significant at the 0.01 level (two-tailed).

deviation and coefficient of variation is presented in Table 5 for PED and MED. From these statistics it may be observed that the variations introduced in the independent variables of the experimental plans allow covering a wide range of pastes and mortars with regard to the fresh and hardened states. For example, in the case of the mortar experimental design, $D_{flow,mortar}$ ranged from 101.8 to 344.0 mm, $T_{funnel,mortar}$ between 2.87 to 38.08 s, fc_{28d} between 79 to 93 MPa and $\rho_{28d,mortar}$ between 49 to 337 Ω m.

3.2. Empirical vs. rheological paste test results

The characterization and control of fresh state behaviour of SCC is critical for the final quality of the structure, and it is usually performed through some empirical tests such as the slump flow or the V-funnel. Although these methods are relatively inexpensive and practical to use in the field, the most accurate way to describe the behaviour of fresh concrete is through rheological tests. The use of rheometers or viscometers allow a quantitative characterization of the material behaviour in terms of fundamental physical measures, less dependent on the details of the apparatus and on the experience and ability of the operator for their implementation and interpretation [10]. A rheological test is an excellent method to characterize cement-based materials since it describes the fresh properties with at least two parameters, i.e., yield stress and plastic viscosity, in contrast to e.g., the slump test which measures the flow of a fluid under a single set of conditions (one point test) [30]. However, rheological test methods have some drawbacks, namely that they are more expensive, require a careful experimental procedure, are rather time consuming and not suited to use at construction sites. Given the advantages and limitations of empirical and rheological tests it is important to find suitable workability test methods for continuous use in the field, and calibrate them with rheological parameters [31–33].

In order to verify if the different test results obtained on pastes correlate with each other, in particular, empirical and rheological test results, a correlation matrix with the Spearman's correlation coefficient was computed (see Table 6). Spearman's correlation coefficient ($\rho_{Spearman}$) is a non-parametric correlation coefficient that determines the degree to which a monotonic relationship exists between two variables (coefficient ranges between −1 and 1). This coefficient does not require the assumption that the relationship between variables is linear and is less sensitive to asymmetries or presence of outliers. It is important to note that if there is a strong correlation between two variables (absolute value of $\rho_{Spearman}$ is close to 1) merely indicates that variables are associated, not implying that one variable causes another [34].

Spearman's correlation coefficients presented in Table 6 indicated on one hand that the empirical test results are related to each other to some degree, the $\rho_{Spearman}$ of spread flow ($D_{flow,paste}$) against free water results (w_{free}) was −0.858 with a significance at the 0.01 level, and, on the other hand, a strong relation was found between empirical and rheological tests. The highest correlation was found between free water results (w_{free}) and plastic viscosity at 10 min ($\eta_{pl,10min}$) with a $\rho_{Spearman}$ of −0.965. In fact, empirical tests, to some extent, provide information about rheology, and this has been shown by many investigators. Several analytical models have been developed to relate slump, as well as spread flow (of concrete, mortar or paste) to yield stress [32,35], but more recent studies seem to indicate that, especially at low viscosity, the final spread diameter is controlled by both yield stress and plastic viscosity [36,37]. According to Roussel and Le Roy [38] the flow time of fresh paste tested in the Marsh cone can be directly linked to plastic viscosity and yield stress for Bingham fluids, which is a simple approximation of the fresh cement paste behaviour. The Spearman's correlation coefficient computed with the data collected in the present work supports these conclusions. Actually $D_{flow,paste}$ and w_{free} have a strong relation with plastic viscosity but also with yield stress (see Table 6). Similar correlation coefficients were found between empirical and rheological tests performed at 10 and 23 min.

It is also noteworthy the relation found between paste electrical resistivity at 28 days and fresh paste properties (empirical and rhe-

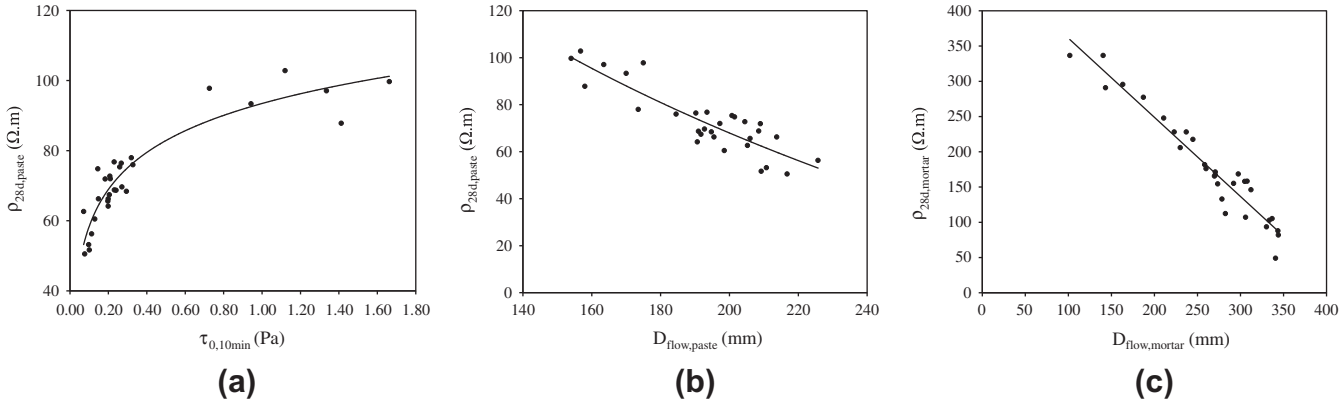

Fig. 3. Relation between (a) $\tau_{0,10min}$ and $\rho_{28d,paste}$ ($\rho_{Spearman} = 0.882$); (b) $\boldsymbol{D_{flow,paste}}$ and $\rho_{28d,paste}$ ($\rho_{Spearman} = -0.810$); (c) $D_{flow,mortar}$ and $\rho_{28d,mortar}$ ($\rho_{Spearman} = -0.956$).

ological), especially with yield stress and spread flow ($\rho_{Spearman} = 0.882$ and $\rho_{Spearman} = -0.810$ for $\tau_{0,10min}$ and $D_{flow,paste}$, respectively) see Table 6, Fig. 3a and b. A strong correlation between resistivity and spread diameter was also found from the results collected in the mortar experimental plan, with a $\rho_{Spearman}$ of −0.956 (see Fig. 3c).

3.3. Time-dependent rheological behaviour of cement pastes

In order to assess the differences in the paste rheological behaviour during the hydration process, two rheological tests were performed in the PED, at 10 and 23 min. The experimental results presented in the graphs below, show that yield stress (Fig. 4) and plastic viscosity (Fig. 5) measured at 23 min are higher than those measured at 10 min. As expected, this time-dependent behaviour is markedly more evident in yield stress than in plastic viscosity. For the range of paste mixtures studied in this PED, yield stress in some cases increased almost 6 times, whereas plastic viscosity increased less than 1.6 times. Early cement hydration increases both, yield stress and plastic viscosity, but it is yield stress that is particularly sensitive to hydration and its associated microstructural changes. The increase in paste yield stress reflects both, the attractive colloidal forces between the cement and other submicron particles that cause them to flocculate, as well as the strength of these attractive interparticle forces [39–41].

In cementitious materials, a reversible rheological behaviour is often observed during the dormant period of the hydration process. As long as the available mixing power is sufficient to break the chemical links between cement particles, the hydration process has a reversible macroscopic time-dependent behaviour referred to as thixotropy [42,43]. Thixotropy is a reversible macroscopic phenomenon which is associated to reversible physico-chemical phenomena such as colloidal flocculation and de-flocculation of the cement particles in combination with the structural breakdown of the chemically formed linkages between the particles [43–45]. However at a microscopic scale, it is a nonreversible chemical reaction that can create new bonds between particles, as long as the reservoir of chemical species is sufficient [43]. Besides the reversible time-dependent behaviour (thixotropy), cementitious materials also show a time-dependent irreversible behaviour. As stated before, in rheological tests performed in this experimental programme, thixotropy effects were mitigated by appropriate pre-conditioning of samples and shear stepped tests, therefore the observed differences in τ_0 and η_{pl} between 10 min and 23 min, corresponds mainly to the irreversible time-dependent behaviour of cement paste. This irreversible rheological transient behaviour observed in suspensions subjected to chemical

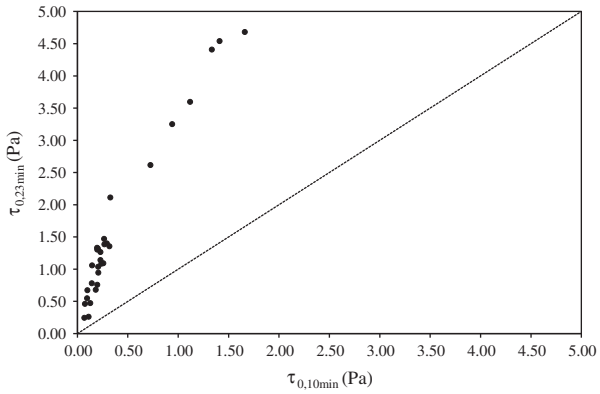

Fig. 4. Relation between the measured at 10 and 23 min in paste mixtures of the PED.

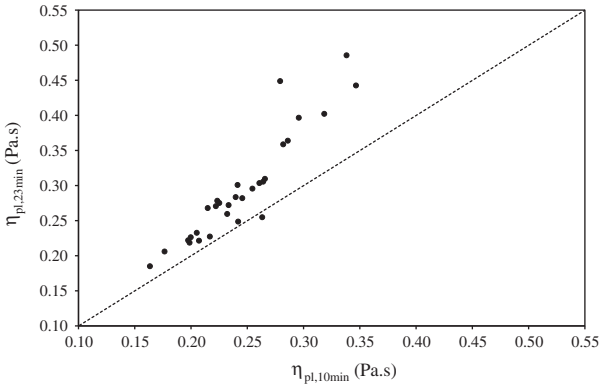

Fig. 5. Relation between the plastic viscosity measured at 10 and 23 min in paste mixtures of the PED.

reactions or particles absorptions is due to concurrent processes like the growth of hydration products and water consumption during cement hydration, the loss of water by evaporation and the loss of dispersing efficiency of the superplasticizer or other water reducing admixtures [36].

4. Response models

In the present study a commercial software [46] was used to analyse the results for each response variable, by examining sum-

mary plots of the data, fitting a model using regression analysis and ANOVA, validating the model by examining the residuals for trends and outliers and, finally, interpreting the model graphically.

4.1. Fitted models

For each response variable, a quadratic model can be estimated from the central composite design data (see Eq. (1) in Section 2.2). The model parameters (β_0, β_i, β_{ij}) are estimated by means of a multilinear regression analysis. It may happen that, for some response variables, some of the terms in Eq. (1) may not be significant. The significance of each factor on a given response can be evaluated using a Student's *t*-test. A backward elimination was used in this work to eliminate non-significant terms in the regression model [46], i.e. those terms associated with a *p*-value greater than the chosen significance level (in this study, $\alpha = 0.05$). The results of the estimated models, including the residual error term, along with the correlation coefficients, are given in Tables 7 and 8, for the PED and MED, respectively.

Notice that the observed values marked with * in Tables 3 and 4 (Section 3) are not typical of the rest of the data. These values were identified as outliers in the statistical analysis and for this reason they have been excluded from the data when fitting the model. Residual analysis did not reveal any obvious model inadequacies or indicate serious violations of the normality assumptions, except in some cases such as $\tau_{0,10min}$ where the problem was overcome after a variable transformation of the form $\log_{10}(y)$, as indicated in Table 7.

4.2. Accuracy of the proposed models

Even though the majority of the fitted models presented considerably high correlation coefficients (see R^2 and $R^2_{adjusted}$ in Tables 7 and 8) their accuracy must be verified. The results of the central points included in the experimental design were analysed in order to estimate the experimental error and the accuracy of the derived models. The corresponding minimum, maximum and mean value, standard deviation and coefficient of variation for PED and MED are presented in Table 9. The estimated residual standard deviation (see Tables 7 and 8) does not exceed the experimental error by far, so a good fitting can be expected.

It must be stressed that the highest coefficients of variation of the central points were associated to $\tau_{0,10min}$ and $\tau_{0,23min}$, 10.4% and 11.7%, respectively. The yield stress was determined by the extrapolation of experimental shear stress vs. shear rate data to zero shear rate, using a numerical fitting to the Bingham model. In fact, the yield stress value obtained by this extrapolation technique is obviously more sensitive to small deviations of the shear stress measured values, which may explain the higher coefficient of variation.

4.3. Individual and interaction effects

Based on the derived models, the relative influence of each variable on the response variation was computed and is presented (in brackets) in Tables 7 and 8 for PED and MED, respectively. Naturally, higher values indicate greater influence of this parameter in the response and on the other hand, a negative value reflects a response decrease to an increase in this parameter. The results clearly show that w/c and mtk/c exhibited a great effect on all measured responses, being the only exception fc_{28d} of MED where the relative influence of mtk/c does not exceed 10%. It should be noted, however, that these two variables have opposite effects on the response. In the case of $\rho_{28d,paste}$ and $\rho_{28d,mortar}$, the variable mtk/c explains almost 50% of the variation of these responses. The partial replacement of cement by a pozzolanic material, like metakaolin, causes substantial changes on the pore structure of the paste and on the chemistry of the hydration products. Metakaolin contributes to the microstructure improvement by the filler effect (like limestone filler) and by the pozzolanic reaction of metakaolin with calcium hydroxide, and this is reflected in the resistivity values. According to some authors, although total porosity may be increased by metakaolin blending, the partial replacement of cement with metakaolin also causes a refinement of pore structure [47]. Metakaolin modifies the pore structure of the cement matrix and significantly reduces permeability, resulting in higher resistance to transportation of water and diffusion of harmful ions which lead to the deterioration of the matrix [48].

Besides w/c and mtk/c, the variable that most influenced w_{free}, $\eta_{pl,10min}$ and $\eta_{pl,23min}$ on PED and $T_{funnel,mortar}$ on MED, was V_w/V_p. A global analysis of the distribution of the relative influence of each parameter on the variation of the response variables of fresh state

Table 7
Fitted numerical models for response variables from PED (coded variables).

	$D_{flow,paste}$ (mm)	w_{free} (kg/m^3)	$\log_{10}[\tau_{0,10\,min}$ (Pa)]	$\eta_{pl,10\,min}$ (Pa s)	$[\tau_{0,23\,min}$ (Pa)]$^{0.5}$	$[\eta_{pl,23\,min}$ (Pa s)]$^{-0.5}$	$\rho_{28d,paste}$ (Ω m)
Independent term	200.399	63.657	−0.654	0.237	1.035	1.907	72.086
V_w/V_p	3.618 (8%)	5.272 (23%)	−0.076 (−9%)	−0.021 (−19%)	−0.083 (−7%)	0.080 (17%)	−0.739 (−3%)
w/c	10.618 (23%)	6.834 (30%)	−0.253 (−29%)	−0.034 (−30%)	−0.336 (−28%)	0.174 (36%)	−7.759 (−29%)
S_p/p	3.799 (8%)	1.744 (8%)	−0.045 (−5%)	−0.004 (−4%)	−0.072 (−6%)	0.037 (8%)	−0.293 (−1%)
mtk/c	−13.465 (−29%)	−6.360 (−28%)	0.287 (32%)	0.030 (27%)	0.312 (26%)	−0.135 (−28%)	12.556 (46%)
$(V_w/V_p) \times (w/c)$	NS	NS	NS	NS	0.046 (4%)	NS	NS
$(V_w/V_p) \times (S_p/p)$	NS	NS	−0.025 (−3%)	−0.004 (−4%)	−0.040 (−3%)	NS	1.548 (6%)
$(V_w/V_p) \times$ (mtk/c)	4.885 (11%)	NS	−0.024 (−3%)	−0.003 (−3%)	−0.067 (−6%)	NS	NS
$(w/c) \times (S_p/p)$	NS	1.373 (6%)	NS	NS	NS	0.027 (6%)	NS
$(w/c) \times$ (mtk/c)	NS	NS	−0.082 (−9%)	−0.004 (−4%)	−0.082 (−7%)	NS	−2.912 (−11%)
$(S_p/p) \times$ (mtk/c)	NS	NS	NS	NS	NS	NS	NS
$(V_w/V_p)^2$	NS	NS	NS	NS	NS	NS	NS
$(w/c)^2$	−5.835 (−13%)	NS	0.067 (8%)	0.008 (7%)	0.095 (8%)	−0.029 (−6%)	NS
$(S_p/p)^2$	NS	NS	NS	NS	NS	NS	NS
(mtk/c)^2	−3.710 (−8%)	−1.180 (−5%)	0.026 (3%)	0.005 (4%)	0.065 (5%)	NS	1.254 (5%)
Residual error, ε*							
Mean	0	0	0	0	0	0	0
Standard deviation	4.909	1.888	0.044**	0.006	0.051**	0.045[b]	2.980
R^2 / $R^2_{adjusted}$	0.930/0.908	0.966/0.958	0.986/0.980	0.984/0.977	0.988/0.981	0.960/0.949	0.955/0.941

(NS) non-significant terms; (%) relative influence of the variable on the response variation.
* Error term is a random and normally distributed variable and no evidence of auto-correlation was found in the residues.
** corresponding value for $\tau_{0,10min}$, $\tau_{0,23min}$ and $\eta_{pl,23min}$ is 0.045, 0.108 and 0.015, respectively.

Table 8
Fitted numerical models for response variables from MED (coded variables).

	$D_{flow,mortar}$ (mm)	$[T_{funnel,mortar}$ (s)$]^{-0.5}$	fc_{28d} (MPa)	$\log_{10}[\rho_{28d,mortar}$ (Ω m)]
Independent term	278.411	0.382	87.640	2.227
V_w/V_p	−0.021 (0%)	0.038 (15%)	−1.341 (−14%)	−0.010 (−3%)
w/c	27.125 (18%)	0.047 (18%)	−3.222 (−34%)	−0.058 (−16%)
S_p/p	7.438 (5%)	0.005 (2%)	−0.301 (−3%)	−0.004 (−1%)
V_s/V_m	−10.229 (−7%)	−0.026 (−10%)	−0.787 (−8%)	0.022 (6%)
mtk/c	−61.000 (−40%)	−0.094 (−36%)	0.997 (10%)	0.203 (56%)
$(V_w/V_p) \times (w/c)$	NS	NS	NS	NS
$(V_w/V_p) \times (S_p/p)$	NS	NS	NS	NS
$(V_w/V_p) \times (V_s/V_m)$	NS	NS	−0.704 (−7%)	NS
$(V_w/V_p) \times$ (mtk/c)	5.969 (4%)	NS	NS	NS
$(w/c) \times (S_p/p)$	NS	NS	NS	NS
$(w/c) \times (V_s/V_m)$	4.375 (3%)	NS	NS	NS
$(w/c) \times$ (mtk/c)	9.563 (6%)	0.012 (5%)	NS	−0.009 (−3%)
$(S_p/p) \times (V_s/V_m)$	−5.719 (−4%)	−0.012 (−5%)	NS	NS
$(S_p/p) \times$ (mtk/c)	NS	NS	NS	0.008 (2%)
$(V_s/V_m) \times$ (mtk/c)	NS	0.011 (4%)	NS	NS
$(V_w/V_p)^2$	NS	0.006 (2%)	NS	−0.008 (−2%)
$(w/c)^2$	−4.763 (−3%)	NS	NS	0.015 (4%)
$(S_p/p)^2$	NS	NS	−0.539 (−6%)	NS
$(V_s/V_m)^2$	NS	NS	−1.041 (−11%)	NS
(mtk/c)^2	−14.826 (−10%)	−0.009 (−4%)	−0.678 (−7%)	−0.028 (−8%)
Residual error, ε^*				
Mean	0	0	0	0
Standard deviation	8.028	0.014**	1.374	0.013**
$R^2/R^2_{adjusted}$	0.984/0.975	0.979/0.969	0.872/0.817	0.995/0.993

(NS) non-significant terms; (%) relative influence of the variable on the response variation.
* Error term is a random and normally distributed variable and no evidence of auto-correlation was found in the residues.
** Corresponding value for $T_{funnel,mortar}$ and $\rho_{28d,mortar}$ is 1.591 and 5.076, respectively.

Table 9
Statistics of the results for central points from PED and MED.

	Minimum	Maximum	Mean	Stand. deviation	Coeff. of variation (%)
Paste experimental design (n = 6 central points)					
$D_{flow,paste}$ (mm)	191.0	208.5	201.3	6.4	3.2
w_{free} (kg/m^3)	59.25	67.17	63.72	2.77	4.4
$\tau_{0,10min}$ (Pa)	0.197	0.259	0.224	0.023	10.4
$\eta_{pl,10\,min}$ (Pa s)	0.222	0.242	0.234	0.009	3.7
$\tau_{0,23\,min}$ (Pa)	0.946	1.330	1.104	0.129	11.7
$\eta_{pl,23\,min}$ (Pa s)	0.248	0.301	0.275	0.017	6.2
$\rho_{28d,paste}$ (Ω m)	65.6	75.3	70.5	3.49	5.0
Mortar experimental design (n = 5 central points)					
$D_{flow,mortar}$ (mm)	268.3	297.5	275.5	11.1	4.0
$T_{funnel,mortar}$ (s)	6.10	7.31	6.87	0.43	6.3
fc_{28d} (MPa)	86.2	90.2	87.8	1.9	2.2
$\rho_{28d,mortar}$ (Ω m)	165.5	171.3	168.1	2.5	1.5

on PED, has revealed a distribution quite similar to the responses $D_{flow,paste}$, $\tau_{0,10min}$ and $\tau_{0,23min}$, as well as to the responses w_{free}, $\eta_{pl,10min}$ and $\eta_{pl,23min}$. In the mortar experimental plan the variable V_s/V_m had some influence, but w/c e mtk/c remain the most prevalent variables in all measured responses. Significant interaction and quadratic effects were found in all responses. The interaction effects represent, on average, a weight of 13% on the variation of the responses and quadratic terms a weight of 11%.

5. SCC mortar design using paste rheological models

5.1. Influence of paste rheology on the workability of mortar

The influence of the rheology of the cement paste matrix on the workability of fresh mortar can be assessed linking the two experimental designs results. In order to understand this influence, the values of independent variables that define the mixture composition of paste tested in the PED, were used in the mortar fitted numerical models to obtain the corresponding $D_{flow,mortar}$ and $T_{funnel,mortar}$. The paste mix-proportions were maintained at the mortar level and only the mixture parameter related with the aggregate skeleton (V_s/V_m) was established. Fig. 6 shows the flow chart used to assess the influence of paste rheology on the workability of mortar.

In Fig. 7a and b the range of rheological parameters, $\tau_{0,10min}$ and $\eta_{pl,10min}$, were plotted against the corresponding mortar workability parameters, $D_{flow,mortar}$ and $T_{funnel,mortar}$, for a $V_s/V_m = 0.45$. From these figures it is clear that there is a strong correlation between the parameters that define the fresh behaviour of paste and mortar. It is also noteworthy that, paste mixtures considered within the PED led to a wide range of mortars in the fresh state, with $D_{flow,mortar}$ ranging between 328 mm and 216 mm and $T_{funnel,mortar}$ ranging between 5.4 s and 16.0 s, for a $V_s/V_m = 0.45$.

The same procedure was performed for V_s/V_m values from 0.40 to 0.50, and the results are presented in Fig. 8. For each paste mixture, the flow properties were described by the ratio of the rheological parameters ($\tau_{0,10min}/\eta_{pl,10min}$) and the workability of the

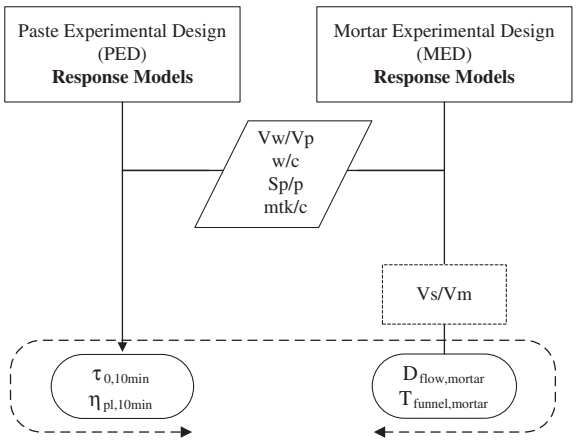

Fig. 6. Flow chart used to assess the influence of paste rheology on the workability of mortar.

corresponding mortar defined as the ratio of the empirical parameters ($D_{flow,mortar}/T_{funnel,mortar}$). As observed in the previous figures, for each V_s/V_m there is a clear correlation between fresh properties of paste and mortar. As V_s/V_m used in mortar increases, the trend line shifts in the direction of lower values of the $D_{flow,mortar}$ to $T_{funnel,mortar}$ ratio. Observing, for example PCC8, one can conclude that mortars with lower aggregate content exhibited a greater ratio (247.2 mm/10.28 s, with $V_s/V_m = 0.40$), while mortars with higher aggregate content showed a lower ratio (194.4 mm/20.26 s, with $V_s/V_m = 0.50$), see Fig. 8.

In fact, increasing $\eta_{pl,10min}$ increases the value of $T_{funnel,mortar}$, at an increasing rate of V_s/V_m, and increasing $\tau_{0,10min}$ decreases the value of $D_{flow,mortar}$, at an increasing rate of V_s/V_m. Similar results were also found by Ferrara et al. [49], when trying to establish correlations between fresh properties of paste (paste mini-cone flow and paste viscosity), the average size and spacing of the solid skeleton particles and the fresh behaviour of the concrete (concrete slump flow and time needed to reach a 500 mm diameter spread, T_{50}). According to these authors, increasing the paste viscosity increases the value of T_{50} in concrete, and decreasing paste mini-cone flow (higher yield stress values) decreases concrete slump flow, at decreasing rate of average aggregate spacing (increasing rate of aggregate content).

5.2. Self-compacting zone at paste level

After building the regression models that establish relationships between mix design variables and the responses (see Section 4), a numerical optimization technique was used to determine the range of mortar mixture parameters where deformability and vis-

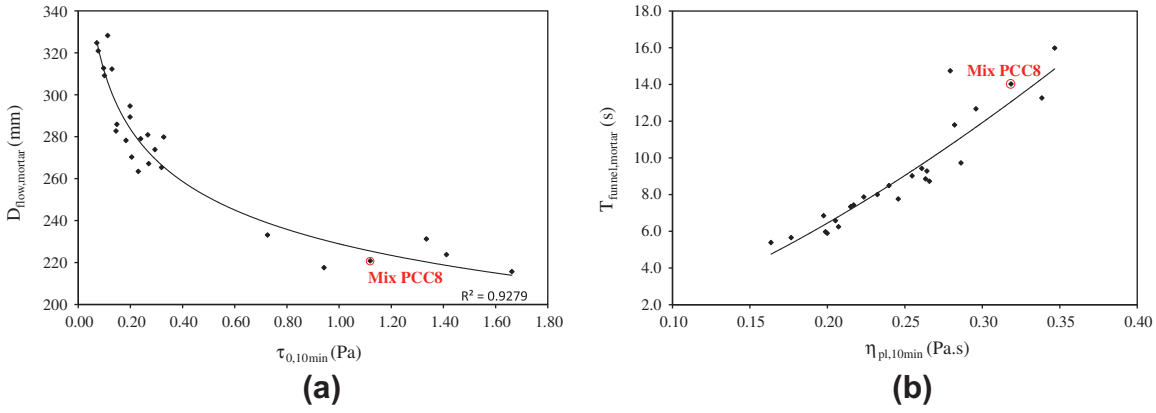

Fig. 7. Relation between: (a) $\tau_{0,10min}$ measured in paste and $D_{flow,mortar}$; (b) $\eta_{pl,10min}$ measured in paste and $T_{funnel,mortar}$, for $V_s/V_m = 0.45$.

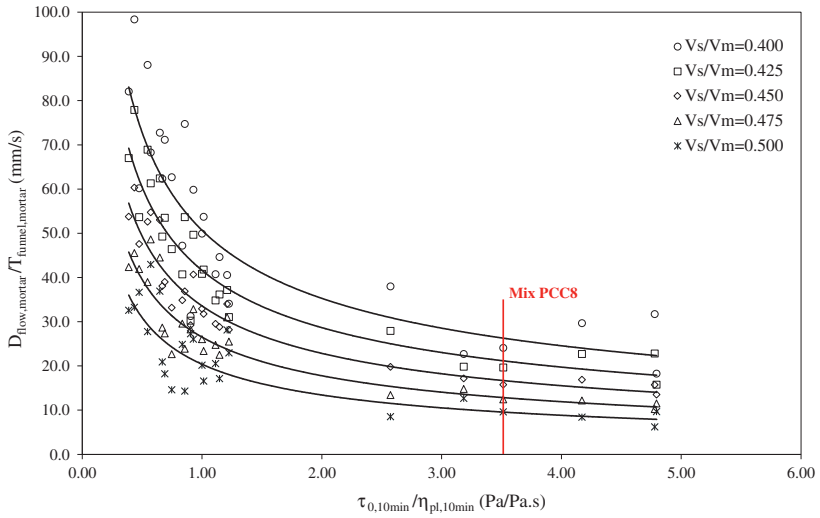

Fig. 8. Relation between fresh properties of paste and mortar, for various V_s/V_m.

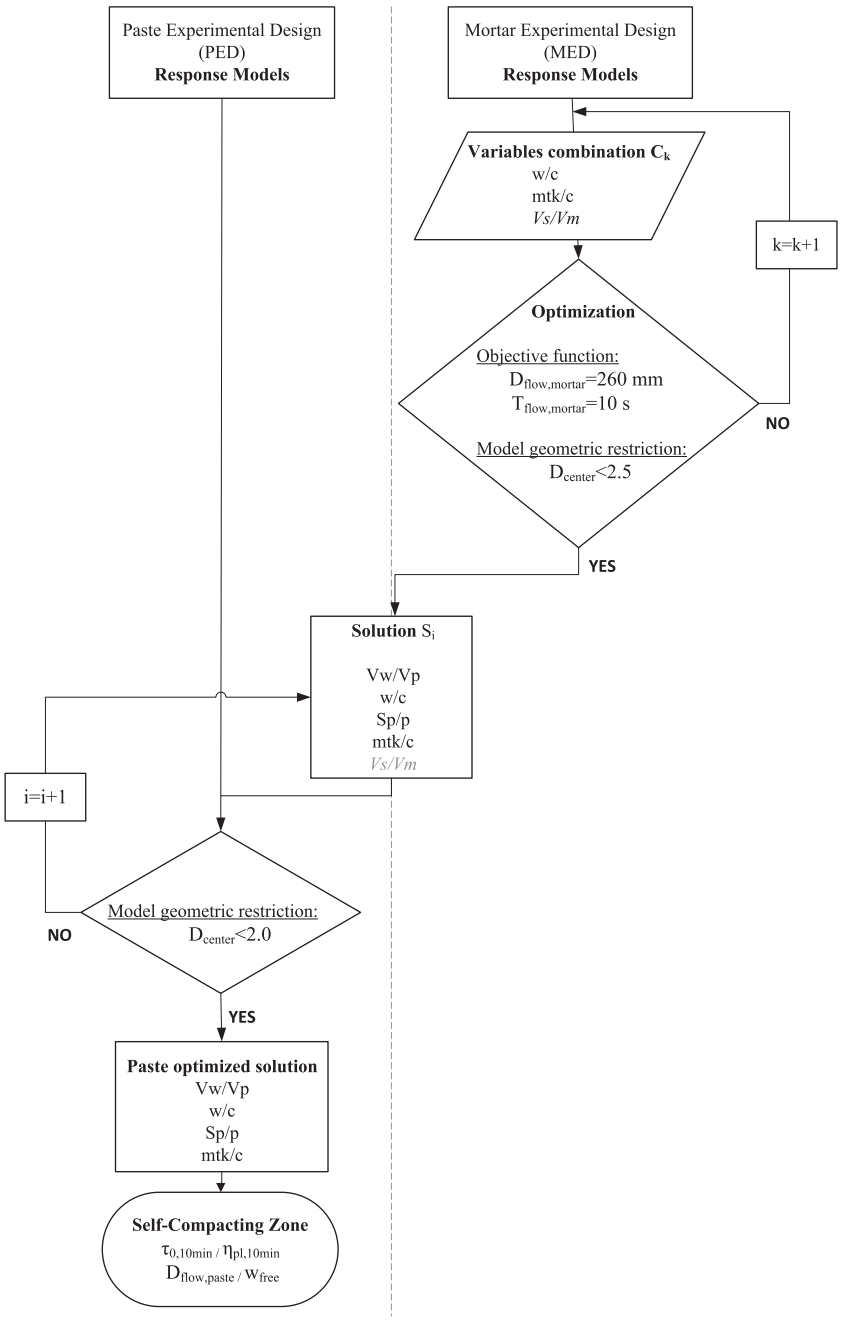

Fig. 9. Flow chart used to determine fresh properties of paste to achieve SCC mortar ($D_{flow,mortar}$ = 260 mm and $T_{funnel,mortar}$ = 10 s).

cosity coexist in a balanced manner to achieve self-compacting mortar, i.e. to determine the best mixtures which exhibit a spread flow of 260 mm and a flow time of 10 s. Mortar fresh requirements that lead to self-compacting concrete were defined based on the values recommended by the Japanese SCC-design method [2], the European Guidelines for SCC [1] and previous experience of other authors [50]. In the present work, a slightly higher target spread flow value was adopted, when compared to the value recommended by the Japanese SCC-designing method (245 mm).

Numerical optimization was performed using a software developed on MATLAB 2011b, which is based on a subroutine provided by the program in the Optimization Toolbox Solvers [51]. In fact, this optimization process is a general problem of solving a system of nonlinear multidimensional equation, with the same number of equality conditions as variables in the model. To solve this system of equations a practical variant of the Newton method was used, in which trust-region modifications to the steps were applied and a preconditioned conjugate gradient method was also used to improve the convergence and simplify the optimization process [52] [51]. The values of V_w/V_p and S_p/p that lead to the optimum mixtures in fresh state ($D_{flow,mortar}$ = 260 mm and $T_{funnel,mortar}$ = 10 s), were searched for each combination of (w/c, mtk/c, V_s/V_m). Note that since the response models were expressed as a function of five independent variables, a multiple optimum will hardly occur. A last constraint should be implemented in the optimization process due to the fact that the error function that is associated to each response model increases with the distance to the center of the modelled region. Therefore, only solutions with a distance to the center of the modelled region (D_{center}) less than 2.5, defined in coded values, were accepted (see Fig. 9).

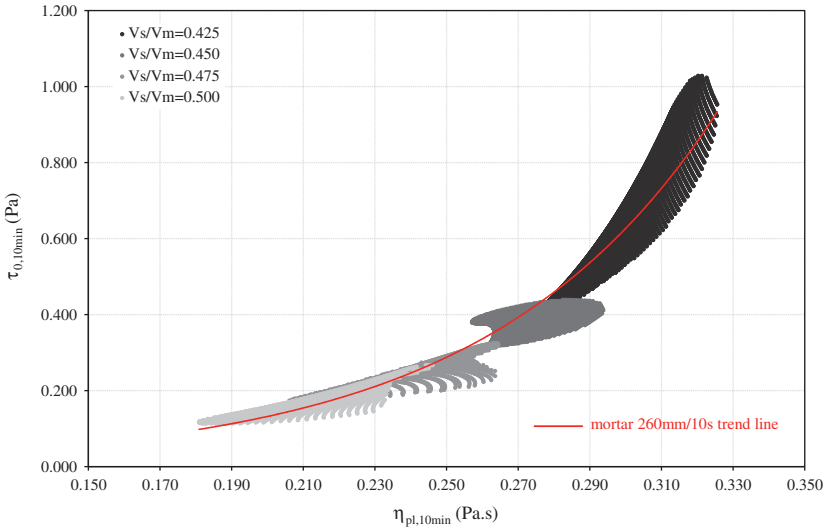

Fig. 10. Rheological properties of paste mixtures to achieve SCC mortars ($D_{flow,mortar}$ = 260 mm and $T_{funnel,mortar}$ = 10 s).

The range of paste mixtures that lead to compositions with self-compacting properties are established from the mortar optimized mixtures (solutions S_i with variables defined in real values). Using the mixture parameters of optimized solutions, the corresponding paste fresh properties were determined using the fitted numerical models from PED. In the same way as performed with mortar models, the use of the paste models was limited to an area bounded by coded values −2.0 to +2.0 (D_{center} < 2.0, see Fig. 9), ensuring that the error in predicting the responses is not relevant. The rheological properties ($\tau_{0,10min}$ and $\eta_{pl,10min}$) of the optimized paste mixtures are plotted in Fig. 10. The results are grouped according to the aggregate content (V_s/V_m) of the mortars that gave rise to paste optimized solutions.

According to these results, higher aggregate contents (V_s/V_m), which correspond to a shorter average distance between aggregate particles, demands a paste with lower yield stress and lower plastic viscosity (more fluid paste), to achieve self-compacting mortars, while lower aggregate contents require a paste with higher yield stress and viscosity (more viscous paste). Therefore, the rheological properties of the paste (yield stress and viscosity) have to be optimized with respect to aggregate content to obtain mortar with the desired flowability and stability characteristics. Indeed, these conclusions meet the fundamentals of the "Excess Paste Theory" proposed by Kennedy in 1940 [53] and applied by Oh et al. [53] to SCC. This theory explained the fact that to reach sufficient workability, it is necessary to have not only enough cement paste to fill all the spaces between the particles, but a volume of cement paste that ensures a very thin lubricating layer around the particles, by virtue of which the friction between the particles is greatly reduced. This cement paste excess layer lubricates the relative movement of the aggregate particles, but also increases flowability of the mixture. Fig. 11 shows the formation of the cement paste excess layer around the aggregate particles. In fact, the characteristics of SCC in the fresh state are affected by two factors: first, the rheological properties of cement paste, and second, the "relative" layer thickness, a parameter proposed by Oh et al. [53] that depends on the excess paste volume and the diameter and surface area of the aggregate. It can however be noted that the cement paste layer thickness is in fact another way to express the average distance between aggregate particles, which is directly related to the aggregate volume fraction. This means that in a mortar with a given workability, as the aggregate volume fraction (V_s/V_m) increases, the paste layer thickness around aggregate decreases, and this

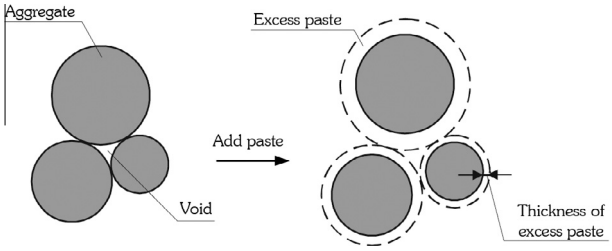

Fig. 11. Excess paste theory [53].

reduction must be balanced with an increase in the paste flowability (lower yield stress and plastic viscosity) to ensure the same workability.

According to Fig. 10, for a given aggregate content (V_s/V_m) it is possible to achieved self-compacting mortar from paste with different rheological properties, i.e., there are different combinations of $\tau_{0,10min}$ and $\eta_{pl,10min}$ that can ensure the desired workability in mortar. However $\tau_{0,10min}$ and $\eta_{pl,10min}$ cannot be varied independently, whereas for this set of materials, paste rheological properties should vary according to the trend line drawn in Fig. 10 to ensure self-compacting mortar (in this case mortar with 260 mm and 10 s). The shape of the trend line reflects the need of compromise between yield stress and plastic viscosity, which seems to indicate that the increase in aggregate content decreases the $\tau_{0,10min}$ to $\eta_{pl,10min}$ ratio and also decreases the influence of the plastic viscosity on the workability of the mortar as compared to yield stress. Similar conclusions can be found if, instead of rheological variables, empirical variables are used, in this case $D_{flow,paste}$ and w_{free}, see Fig. 12. In fact others authors, using a different methodology, have reached similar conclusions [12]. Bui et al. [12] developed a segregation-controlled design methodology for SCC based on the paste rheology criteria, which include minimum apparent viscosity, minimum slump flow diameter, and optimum slump flow diameter to viscosity ratio. According to these authors the optimum slump flow diameter to viscosity ratio of paste is related to the average aggregate diameter and aggregate spacing (aggregate content), where higher aggregate spacing requires lower slump flow diameter to viscosity ratio.

Specifications of fresh SCC properties should depend on the type of application and on requirements such as, confinement conditions, placing equipment, placing method or finishing method

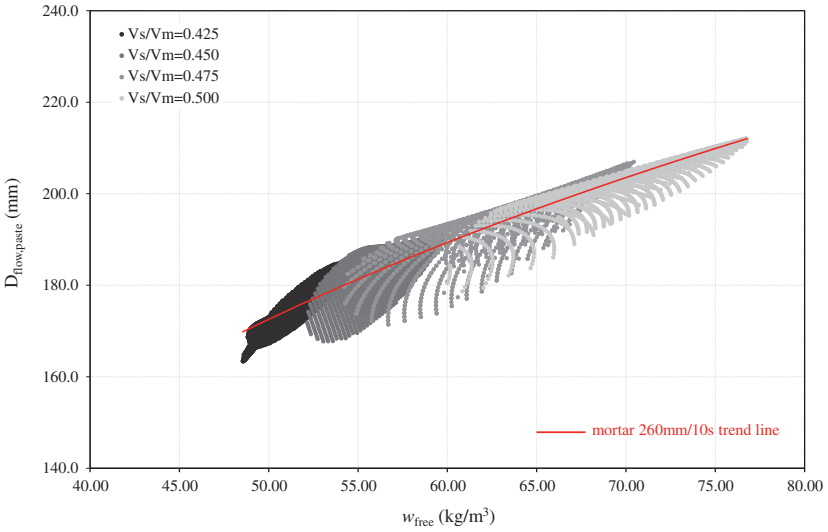

Fig. 12. Empirical fresh properties of paste mixtures to achieve SCC mortars ($D_{flow,mortar}$ = 260 mm and $T_{funnel,mortar}$ = 10 s).

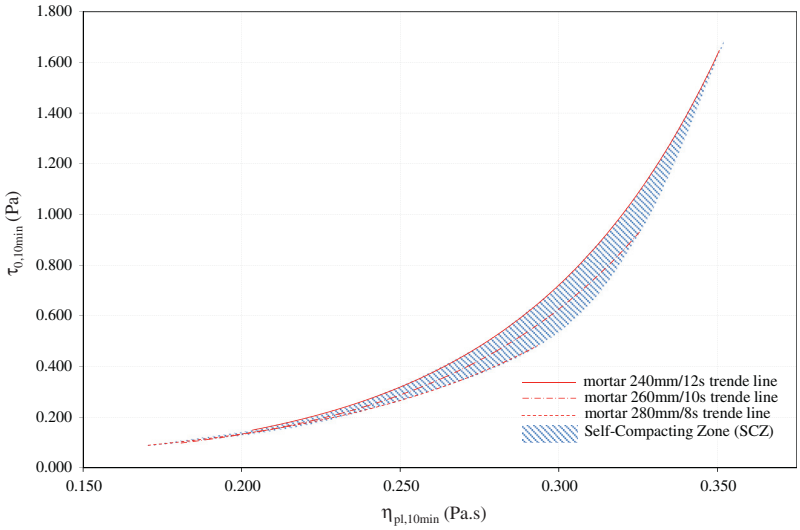

Fig. 13. Self-compacting zone at paste level (SCZ) for the set of materials used in this study.

[54]. A low SCC viscosity may be of interest when good surface finish is required, while a viscous SCC with lower slump flow and higher funnel time is more appropriate to be used under a strong inclination such as ramps in parking houses. Indeed, based on these borderline situations, in terms of fresh SCC properties it is possible to establish a self-compacting zone. Applying the procedure described above to both situations, a very fluid self-compacting mortar (e.g. a mortar with $D_{flow,mortar}$ = 280 mm and $T_{funnel,mortar}$ = 8 s) and a very viscous self-compacting mortar (e.g. a mortar with $D_{flow,mortar}$ = 240 mm and $T_{funnel,mortar}$ = 12 s), the respective trend lines can be computed as illustrated in Fig. 13, which allows to define a self-compacting zone at paste level (SCZ), for the set of materials used in this study.

This SCZ has a great applicability in producing SCC, since it allows an expeditious design of mortar mixtures, and therefore of concrete, with the desired self-compacting properties. This design approach can simplify the test protocol required to optimize a given SCC mixture, namely, to select the combination of powder materials with admixtures and to design tailor-made and economic SCC mixtures. It should be mentioned that this SCZ will probably change if a different set of materials is used (addition, superplasticizer or viscosity agent). In fact, studies conducted by Saak et al. [11], allowed to conclude that there is a variation in the relative size and position of the SCZ for a different set of materials. The effect of a new admixture or a new superplasticizer could be assessed at the paste level based on this SCZ although demanding some adjustments at mortar level, which may be required to achieve the final mortar mixture.

5.3. Mixture proportions of optimized SCC mortar

The adjusted values of mtk/c and S_p/p for each pair of (w/c, V_w/V_p) were used to obtain the contour plots presented in Fig. 14. The mixtures which exhibit a spread flow of 260 mm and a flow time of 10 s are marked with small (+). This figure shows that the increase in sand content led to an adjustment of the variable range where SCC mortars can be found, namely, the range of w/c and V_w/V_p move to higher values and the range of mtk/c move to lower values.

After selecting the paste mix proportions, a SCC concrete mixture can be achieved substituting reference sand (sand used in this study) by real aggregates, fine and coarse aggregate). Tests on concrete are then necessary to optimize the aggregate skeleton and

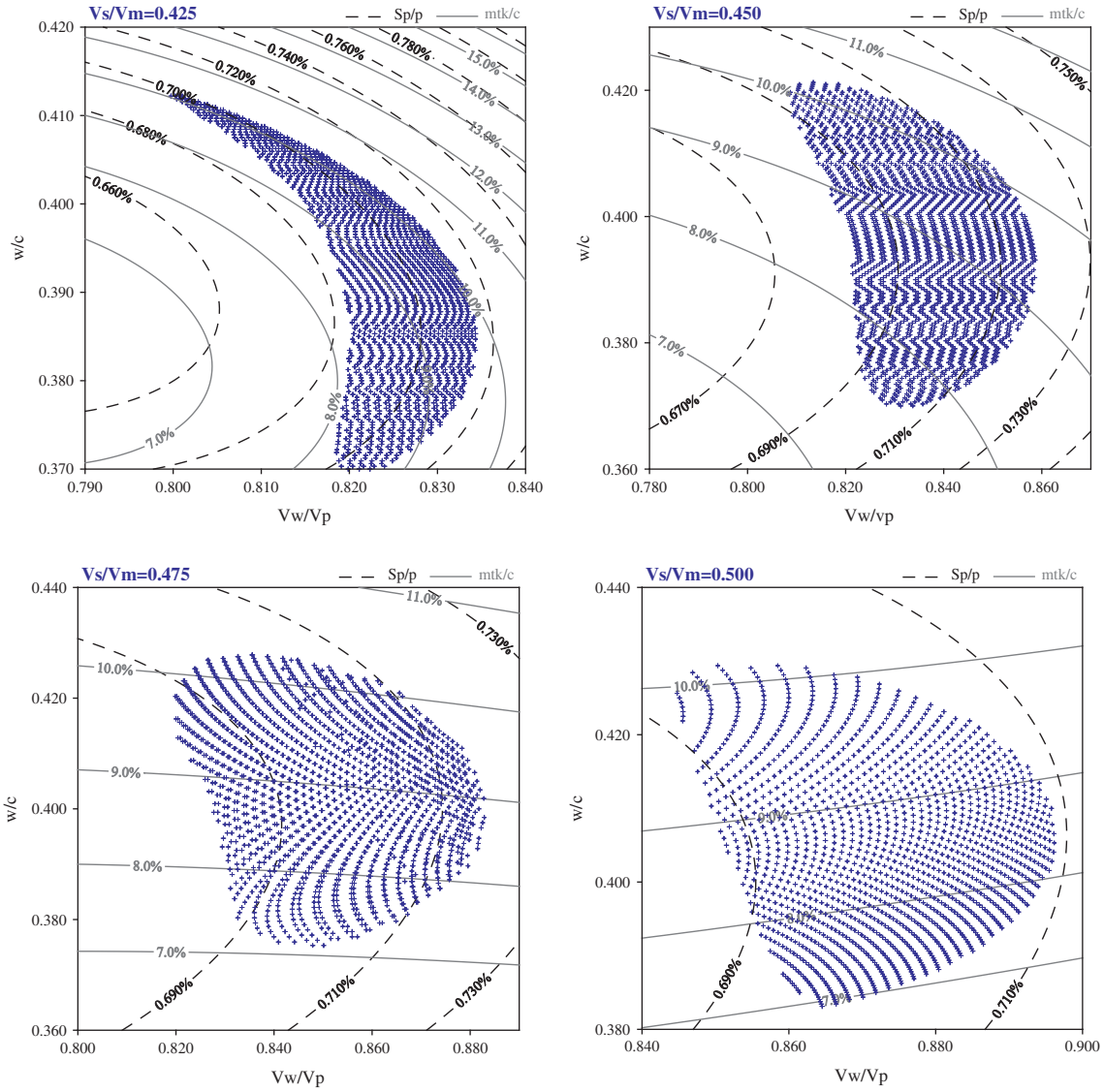

Fig. 14. Range of mixture variables (absolute values) for optimized mortars, marked with (+) ($D_{flow,mortar}$ = 260 mm and $T_{funnel,mortar}$ = 10 s).

aggregate content. Paste mixtures corresponding to a higher sand content (V_s/V_m) in the optimized mortar mixtures can lead to SCCs with higher total aggregate content and lower paste volume, thus resulting in more economic mixtures [50]. On the other hand, increasing the paste volume increases mixture robustness and allows the accommodation of poorly graded or poorly shaped aggregates [55].

6. Influence of aggregate content on the electrical resistivity

With the purpose of evaluating the influence of aggregate on electrical resistivity, the correlation between paste and mortar resistivity was assessed, for different aggregate contents. The correlation was obtained based on the results provided by paste and mortar fitted models (see Section 4), applied to the experimental mixtures carried out on the paste experimental design (PED). Fig. 15 shows the electrical resistivity results for paste mixtures and respective mortars with different aggregate contents, as well as the respective trend line. For each V_s/V_m a good correlation between paste and mortar resistivity was found, following a linear trend line with a correlation coefficient above 0.96. The trend line slope increases as more aggregate are added to the paste, which means that the aggregate contributes to increase mixture resistivity.

Indeed, the inclusion of aggregates in the cement paste matrix has an effect of dilution (blocking) and tortuosity (redirecting). The dilution effect depends on the aggregate volume fraction, and it occurs because the aggregate conductivity (inverse of resistivity) is much lower compared with the cement paste conductivity. Paste electrical conductivity ($\sigma_{paste} = 1/\rho_{28d,paste}$) is affected by the dilution effect, according to the Eq. (6):

$$\frac{\sigma_{mortar}}{\sigma_{paste}} = (1 - V_s/V_m) \tag{6}$$

where σ_{mortar} $(1/\rho_{28d,mortar})$ is the electrical conductivity of the mortar. The tortuosity effect occurs due to the presence of these "insulating" elements, the aggregate particles, forcing a redirection of conduction around them, making the conduction paths more tortuous.

The effect of including aggregates in the cement paste matrix can be predicted by the Differential Effective Medium Theory (D-EMT), also called asymmetric Bruggeman formulation. For the case of a two-phase mixture (cement paste and aggregate), of not diluted dispersion of insulating spherical inclusions (aggregate) the

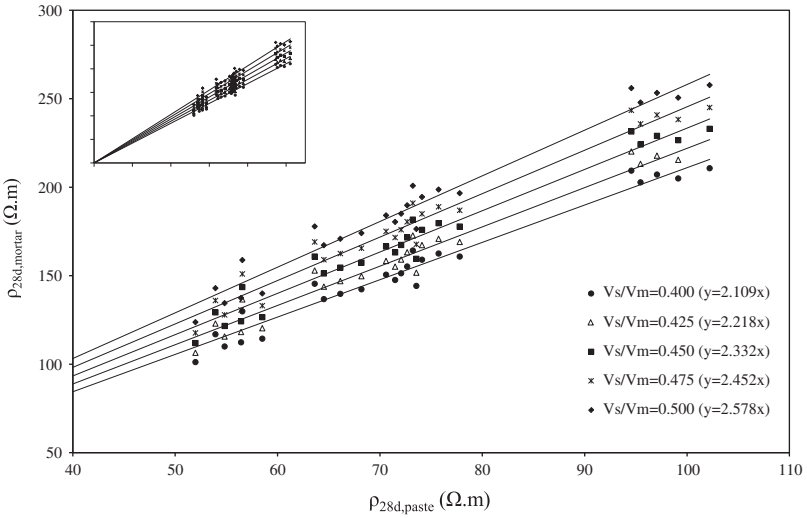

Fig. 15. Relation between paste and mortar electrical resistivity as a function of V_s/V_m.

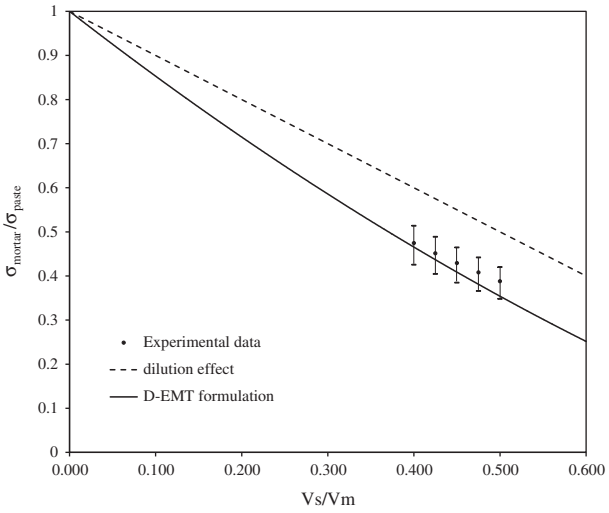

Fig. 16. Comparison of experimental results with D-EMT formulation.

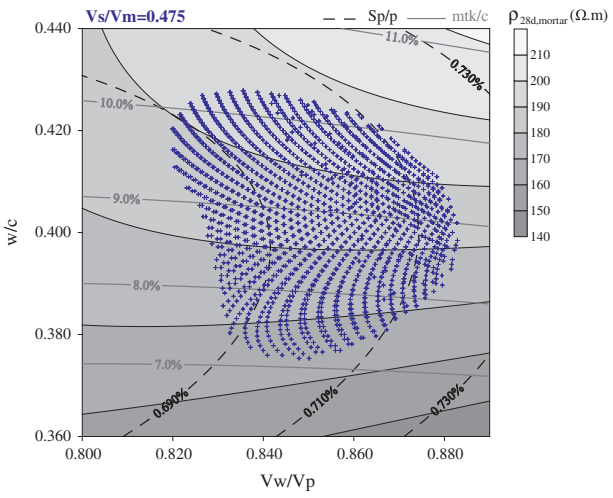

Fig. 17. Optimized mixture parameters for SCC mortars, marked with (+) ($D_{flow,mortar}$ = 260 mm; $T_{funnel,mortar}$ = 10 s; V_s/V_m = 0.475), and estimated values of $\rho_{28d,mortar}$.

D-EMT formulation leads to the formula presented in Eq. (7). This model also assumes that the inclusion of spherical particles (aggregate) does not change the matrix electrical conductivity (paste).

$$\frac{\sigma_{mortar}}{\sigma_{paste}} = (1 - V_s/V_m)^{3/2}. \quad (7)$$

In Fig. 16 the $\sigma_{mortar}/\sigma_{paste}$ results are plotted as a function of the volume fraction of aggregate, and are compared with the theoretical equations that express the dilution effect (Eq. (6) and both the dilution and tortuosity effect (Eq. (7)).

Comparing the average value of the experimental data with the theoretical models it seems that the main effect of adding more sand is blocking and redirecting conductive flow. Average values of the experimental data are very close to the $(1 - V_s/V_m)^{3/2}$ power line law. However, although in the vicinity, the results are always above the line and the distance appears to increase as more aggregate is added to paste. Indeed, the presence of aggregate in a cement paste matrix has two opposite effects on the transport properties: firstly, the dilution and tortuosity effects that reduce the permeability, secondly, the presence of a porous interfacial transition zone (ITZ) between paste and the aggregate that facilitates the movement of ions and increases mortar conductivity ([56] [57]). The volume and properties of the ITZ are influenced by the *w*/*c* ratio, addition of pozzolanic or inert fine particles, aggregate volume fraction or the stability of fresh mix. In the presence of low *w*/*c* ratios or fine mineral addition, like in SCC, some studies appear to indicate that the porosity and width of the ITZ is significantly smaller than in vibrated concrete. Furthermore, the ITZ formed around the aggregate increases locally the *w*/*c* ratio, but this is usually accompanied by a decrease in *w*/*c* ratio of bulk matrix, and therefore a decrease in the conductivity because of the lower porosity ([56] [57]). Another aspect that should be taken into consideration is the fact that the model presented in Eq. (7) considers spherical aggregate, but in fact, aggregates shape could be more ellipsoidal or the aggregates could packed in clusters that behave as individual ellipsoids.

Once established this link between paste and mortar, it is possible to design mortar mixtures with the desired resistivity requirement, by simply conducting some trials at paste level. In Fig. 17 the mortar resistivity predictions were added to the contour plot presented in Fig. 14 (Section 5) for a V_s/V_m = 0.475, allowing to

simplify the test protocol required to optimize a given self-compacting mortar mixture with the desired durability requirement (resistivity). Although not presented in this work, it is important to emphasize that this link could be extended to the concrete level.

7. Conclusions

Based on the results presented in this paper, the following conclusions can be drawn:

1. Empirical tests performed in paste ($D_{\text{flow,paste}}$ and w_{free}) correlate with the rheological parameters of paste, namely, yield stress and plastic viscosity, which seems to indicate that both types of tests can be used to characterize paste fresh behaviour.
2. Rheological tests performed at 10 min and 23 min, after starting of mixing, showed that paste rheological behaviour evolves from very young ages (time-dependent behaviour). Early cement hydration increase both, yield stress and plastic viscosity, but it is yield stress that is particularly sensitive to hydration reaction and their associated microstructural changes.
3. Data collected during the experimental plan, conducted according to central composite design, can be used to establish numerical models relating mixture parameters with fresh and hardened properties of paste and mortar. Such numerical models provide an effective means to design paste and mortar mixtures by determining the influence of key parameters on the desired fresh and durability properties.
4. A link between fresh properties of paste and SCC mortar was established using paste and mortar fitted numerical models. Fresh properties of paste (rheological and empirical) have to be optimized with respect to aggregate content to obtain mortar with the desired flowability and stability characteristics. For a given aggregate content it is possible to achieved SCC mortar from paste mixtures with different rheological properties, however yield stress and plastic viscosity cannot be varied independently. For given mortar target properties ($D_{\text{flow,mortar}}$ and $T_{\text{funnel,mortar}}$) a trend line establishing the relationship between paste rheological parameters was computed.
5. The link established between fresh properties of paste and SCC mortar allowed the definition of a self-compacting zone at paste level (SCZ). This SCZ can simplify the test protocol required to optimize a given SCC mixture, reducing the extent of laboratory work, testing time and materials used.
6. Although the SCZ was defined for a specific set of materials, variations in material characteristics are expected to change the relative size of the SCZ. Depending on the level of deviation, a limited number of mixtures can be prepared to adjust the final composition. The SCZ can also provide the basis for quality control and further behaviour assessment of new materials (addition, superplasticizer or viscosity agent).
7. A link between durability properties of paste and SCC mortar was established using electrical resistivity numerical models of paste and mortar. For each V_s/V_m a good correlation between resistivity of paste and mortar was found, showing that aggregate increases mixture resistivity. Comparing experimental data with D-EMT formulation, it seems that the ITZ zone has little influence on the electrical resistivity of SCC mortar and the main effect of aggregate is blocking and redirecting conductive flow.

Acknowledgments

This work was financed by FEDER funds under the Operational Program Factors of Competiveness – COMPETE and by National Funds under FCT – Foundation for Science and Technology through Project PTDC/ECM/098117/2008 – Additions from waste materials for sustainable structural concrete, and supported by FCT PhD research Grant SFRH/BD/25552/2005. The authors would like to sincerely acknowledge the cooperation of Eng. Lino Maia on part of the research work developed.

Appendix A

Mix proportions of paste and mortar prepared in this study were obtained using the following formulation. First, for a defined volume of mortar (V_m), considering equal to 1 cubic meter, and a given value of (V_s/V_m), sand volume (V_s) can be obtained from

$$V_s = V_s/V_m \times V_m = V_s/V_m \tag{8}$$

and for a given value of (V_w/V_p), the powder volume (V_p) and the water volume (V_w) can be defined as

$$V_p = \frac{1 - V_s}{1 + (V_w/V_p)} \tag{9}$$

$$V_w = V_w/V_p \times V_p. \tag{10}$$

Finally, from the V_p and V_w values the weight values of water (w_w), cement (w_c), metakaolin (w_{mtk}) and limestone filler (w_f) can be determined as follows

$$w_w = V_w \times \rho_w \tag{11}$$

$$w_c = \frac{w_w}{w/c} \tag{12}$$

$$w_{\text{mtk}} = \text{mtk}/c \times w_c \tag{13}$$

$$w_f = \left(V_p - \frac{w_c}{\rho_c} - \frac{w_{\text{mtk}}}{\rho_{\text{mtk}}}\right) \times \rho_f \tag{14}$$

where ρ_w, ρ_c, ρ_{mtk} and ρ_f represent the specific gravity of water, cement, metakaolin and limestone filler, respectively. From the superplasticizer dosage (S_p/p) and the weight values of cement, metakaolin and limestone filler the liquid weight of superplasticizer (w_{sp}) is given by

$$w_{\text{Sp}} = \text{Sp}/p \times (w_c + w_{\text{mtk}} + w_f). \tag{15}$$

Dry aggregate content (w_{sd}) can be obtained as follows

$$w_{\text{Sd}} = V_s \times \rho_{\text{sd}} \tag{16}$$

where ρ_{sd} represent the specific gravity of reference sand. The water added to the mixture has to be corrected (w_{wc}) by subtracting the water content of the superplasticizer and adding the water needed for saturating the aggregate, from a dry state, as follows

$$w_{\text{wc}} = w_w - w_{\text{sp}} \times (1 - \gamma_{\text{sp}}) + w_{\text{sd}} \times A_{\text{sd}} \tag{17}$$

where γ_{sp} and A_{sd} represent the solid content of superplasticizer and the absorption coefficient of the reference sand, respectively. For paste mix proportioning the same formulation could be used, considering the sand to mortar volume ratio (V_s/V_m) equal to zero.

References

[1] EFNARC. The European guidelines for self-compacting concrete – specification, production and use. In: BIBM, CEMBUREAU, ERMCO, EFCA, EFNARC, editors. 2005. p. 63.
[2] Okamura H, Ouchi M. Self-compacting concrete. J Adv Concr Technol 2003;1(1):5–15.
[3] Khayat K, Ghezal A, Hadriche M. Utility of statistical models in proportioning self-consolidating concrete. Mater Struct 2000;33(5):338–44.
[4] Nehdi M, Summer J. Optimization of ternary cementitious mortar blends using factorial experimental plans. Mater Struct 2002;35(8):495–503.

[5] Sonebi M. Medium strength self-compacting concrete containing fly ash: modelling using factorial experimental plans. Cem Concr Res 2004;34(7):1199–208.
[6] Nunes S. Performance-based design of self-compacting concrete (SCC): a contribution to enchance SCC mixtures robustness. Universidade do Porto; 2008.
[7] Hidalgo J, Chen C, Struble L. Correlation between paste and concrete flow behavior. ACI Mater J 2008;105(3):281–8.
[8] Grünewald S, Walraven J. Characteristics and influence of paste on the behaviour of self-compacting concrete in the fresh state. In: Schutter GD, Boel V, editors. 5th International RILEM symposium on self-compacting concrete. Ghent, Belgium: RILEM Publications SARL; 2007. p. 137–42.
[9] Roussel N, Lemaître A, Flatt RJ, Coussot P. Steady state flow of cement suspensions: a micromechanical state of the art. Cem Concr Res 2010;40(1):77–84.
[10] Wallevik OH, Wallevik JE. Rheology as a tool in concrete science: the use of rheographs and workability boxes. Cem Concr Res 2011;41(12):1279–88.
[11] Saak AW, Jennings HM, Shah SP. New methodology for designing self-compacting concrete. ACI Mater J 2001;98(6):429–39.
[12] Bui V, Akkaya Y, Shah S. Rheological model for self-consolidating concrete. ACI Mater J 2002;99(6):549–59.
[13] CEN – European committee for standardization. EN 197-1:2011 Cement. Part 1: composition, specifications and conformity criteria for common cements; 2011.
[14] CEN – European committee for standardization. EN 196-1:2005 Methods of testing cement. Determination of strength; 2005.
[15] Montgomery D. Design and analysis of experiments. 5th ed. New York: Wiley; 2001.
[16] Yahia A, Khayat KH. Experiment design to evaluate interaction of high-range water-reducer and antiwashout admixture in high-performance cement grout. Cem Concr Res 2001;31:749–57.
[17] Nunes S, Figueiras H, Oliveira PM, Coutinho JS, Figueiras J. A methodology to assess robustness of SCC mixtures. Cem Concr Res 2006;36(12):2115–22.
[18] Sonebi M. Factorial design modelling of mix proportion parameters of underwater composite cement grouts. Cem Concr Res 2001;31(11):1553–60.
[19] Gomes P. Optimization and characterization of high-strength self-compacting concrete. Universitat Politécnica de Catalunya; 2002.
[20] Grünewald S. Performance-based design of self-compacting fibre reinforced concrete 2004.
[21] Fennis S. Measuring water demand or packing density of micro powders – comparison of methods. Delft University of Technology; 2011.
[22] Nunes S, Oliveira PM, Sousa Coutinho J, Figueiras J. Rheological characterization of SCC mortars and pastes with changes induced by cement delivery. Cem Concr Compos 2011;33(1):103–15.
[23] Yahia A, Khayat KH. Analytical models for estimating yield stress of high-performance pseudoplastic grout. Cem Concr Res 2001;31(5):731–8.
[24] Ferraris C. Concrete rheology: what is it and why do we need it? In: Yu Z, Shi C, Khayat K, Xie Y, editors. In: 1st International symposium on design, performance and use of self-consolidating concrete. China: RILEM; 2005.
[25] Chhabra R, Richardson J. Non-Newtonian flow in the process industries. Fundamentals and engineering applications. Oxford: Butterworth-Heinemann; 1999.
[26] Ltd BI. A basic introduction to rheology. Bohlin Instruments Ltd.; 1994.
[27] Andrade C. Calculation of initiation and propagation periods of service life of reinforcements by using the electrical resistivity. In: Weiss J, Kovler K, Marchand J, Mindess S, editors. First international RILEM symposium on advances in concrete through science and engineering: a tribute to Arnon. Evanston: RILEM Publications SARL; 2004.
[28] Rajabipour F, Weiss J. Electrical conductivity of drying cement paste. Mater Struct 2007;40(10):1143–60.
[29] Shi C, Stegemann JA, Caldwell RJ. Effect of supplementary cementing materials on the specific conductivity of pore solution and its implications on the rapid chloride permeability test (AASHTO T277 and ASTM C1202) results. ACI Mater J 1998;94(4):389–93.
[30] Banfill P. Rheology of fresh cement and concrete. Rheology reviews 2006: The British Society of Rheology; 2006. p. 61–130.
[31] Utsi S, Emborg M, Calswärd J. Relation between workability and rheological parameters. In: Wallevik O, Nielsson I, editors. 3rd International symposium on self-compacting concrete. Reykjavik, Iceland: RILEM publications SARL; 2003. p. 154–64.
[32] Saak A, Jennings H, Shah S. A generalized approach for the determination of yield stress by slump and slump flow. Cem Concr Res 2004;34(3):363–71.
[33] Zerbino R, Barragán B, Garcia T, Agulló L, Gettu R. Workability tests and rheological parameters in self-compacting concrete. Mater Struct 2009;42(7):947–60.
[34] Sheskin DJ. Handbook of parametric and nonparametric statistical procedures. Chapman and Hall; 2003.
[35] Roussel N, Leroy CSR. From mini-cone test to Abrams cone test: measurement of cement-based materials yield stress using slump tests. Cem Concr Res 2005;35(5):817–22.
[36] Esping O. Early age properties of self-compacting concrete. Effects of fine aggregate and limestone filler Ph.D. Sweden: Chalmers University of Technology; 2007.
[37] Bouvet A, Ghorbel E, Bennacer R. The mini-conical slump flow test: analysis and numerical study. Cem Concr Res 2010;40(10):1517–23.
[38] Roussel N, Roy RL. The Marsh cone: a test or a rheological apparatus? Cem Concr Res 2005;35(5):823–30.
[39] Struble LJ, Lei W. Rheological changes associated with setting of cement paste. Adv Cem Based Mater 1995;2(6):224–30.
[40] Struble L, Szecsy R, Salinas G. Rheology of fresh concrete. In: Chong KP, editor. 4th ASCE materials engineering conference proceedings, materials for the new millenium. New York: American Society of Civil Engineers; 1996. p. 1121–8.
[41] Petrou MF, Wan B, Gadala-Maria F, Kolli VG, Harries KA. Influence of mortar rheology on aggregate settlement. ACI Mater J 2000;97(4):479–85.
[42] Saak A. Characterization and modeling of the rheology of cement paste: with applications toward self-flowing materials. Evanston, Illinois: Northwestern University; 2000.
[43] Roussel N, Ovarlez G, Garrault S, Brumaud C. The origins of thixotropy of fresh cement pastes. Cem Concr Res 2012;42(1):148–57.
[44] Roussel N. Steady and transient flow behaviour of fresh cement pastes. Cem Concr Res 2005;35(9):1656–64.
[45] Wallevik JE. Rheological properties of cement paste: thixotropic behavior and structural breakdown. Cem Concr Res 2009;39(1):14–29.
[46] Design-expert-software. Design-expert software. Version 7 User's Guide: State-Ease Corporation; 2007.
[47] Frías M, Cabrera J. Pore size distribution and degree of hydration of metakaolin–cement pastes. Cem Concr Res 2000;30(4):561–9.
[48] Siddique R, Klaus J. Influence of metakaolin on the properties of mortar and concrete: a review. Appl Clay Sci 2009;43(3–4):392–400.
[49] Ferrara L, Park Y, Shah S. A method for mix-design of fiber-reinforced self-compacting concrete. Cem Concr Res 2007;37(6):957–71.
[50] Nunes S, Oliveira PM, Joana Sousa Coutinho, Figueiras J. Interaction diagrams to assess SCC mortars for different cement types. Constr Build Mater 2009;23(3):1401–12.
[51] Optimization Toolbox – User's Guide. MathWorks; 2011.
[52] Nacedal J, Wright S. Numerical optimization. Springer; 2006.
[53] Oh S, Noguchi T, Tomosawa F. Toward mix design for rheology of self-compacting concrete. In: Skarendahl Å, Petersson Ö, editors. First international RILEM symposium on self-compacting concrete. Stockholm: Sweden RILEM Publications SARL; 1999. p. 361–72.
[54] CEN – European committee for standardization. EN 206-9:2010 – Concrete – Part 9: additional rules for self-compacting, concrete (SCC); 2010. p. 35.
[55] Koehler E, Fowler D. Aggregates in self-compacting concrete. Aggregates foundation for technology, research, and education (AFTRE). International Center for Aggregates Research (ICAR) and The University of Texas at Austin; 2007. p. 353.
[56] Durability of self-compacting concrete – state-of-the-art report of RILEM technical committee 205-DSC. In: Schutter G, Audenaert K, editors. RILEM Publications SARL; 2007. p. 208.
[57] Garboczi E, Bentz D, Shane J, Mason T, Jennings H. Effect of the interfacial transition zone on the conductivity of Portland cement mortars. J Am Cermaic. 2000;83(5):1137–44.